frontiers | Frontiers in Immunology

TYPE Original Research
PUBLISHED 24 October 2023
DOI 10.3389/fimmu.2023.1254697

OPEN ACCESS

EDITED BY
Marcus Thelen,
Institute for Research in Biomedicine (IRB), Switzerland

REVIEWED BY
Sergio M. Pontejo,
National Institute of Allergy and Infectious Diseases (NIH), United States
Tamara Girbl,
University of Würzburg, Germany

*CORRESPONDENCE
James E. Pease
j.pease@imperial.ac.uk

RECEIVED 07 July 2023
ACCEPTED 09 October 2023
PUBLISHED 24 October 2023

CITATION
Giblin SP, Ranawana S, Hassibi S, Birchenough HL, Mincham KT, Snelgrove RJ, Tsuchiya T, Kanegasaki S, Dyer D and Pease JE (2023) CXCL17 binds efficaciously to glycosaminoglycans with the potential to modulate chemokine signaling.
Front. Immunol. 14:1254697.
doi: 10.3389/fimmu.2023.1254697

CXCL17 binds efficaciously to glycosaminoglycans with the potential to modulate chemokine signaling

Sean P. Giblin[1], Sashini Ranawana[1], Shyreen Hassibi[1], Holly L. Birchenough[2], Kyle T. Mincham[1], Robert J. Snelgrove[1], Tomoko Tsuchiya[3], Shiro Kanegasaki[4], Douglas Dyer[2,5] and James E. Pease[1]*

[1]National Heart and Lung Institute, Imperial College London, London, United Kingdom, [2]Wellcome Centre for Cell-Matrix Research, Lydia Becker Institute of Immunology and Inflammation, Faculty of Biology, Medicine and Health, Manchester Academic Health Science Centre, University of Manchester, Manchester, United Kingdom, [3]Research Institute, National Center for Global Health and Medicine, Shinjuku-ku, Japan, [4]Heavy Ion Medical Center, Gunma University, Maebashi, Japan, [5]Geoffrey Jefferson Brain Research Centre, Manchester Academic Health Science Centre, Northern Care Alliance NHS Group, University of Manchester, Manchester, United Kingdom

Introduction: CXCL17 is a mucosally secreted protein, and the most recently identified human chemokine, an assignment based on protein fold prediction and chemotactic activity for leukocytes. However, these credentials have been the subject of much recent discussion and no experimental evidence has been presented regarding the definitive structure of CXCL17. In this study, we evaluated the structural and chemoattractant credentials of CXCL17 to better characterize this molecule, and gain deeper insights into its functional role as a glycosaminoglycan (GAG) binding protein.

Methods: In the absence of structural information, *in silico* modeling techniques assessed the likelihood of CXCL17 adopting a chemokine fold. Recombinant CXCL17 was synthesized in mammalian and prokaryotic systems. Modified Boyden chamber and real-time chemotaxis assays assessed the ability of CXCL17 to promote chemotaxis of murine splenocytes, human neutrophils, and CXCR1 transfectants. The efficacy of CXCL17 binding to GAGs was quantified with solid-phase assays and bio-layer interferometry techniques

Results: All modeling efforts failed to support classification of CXCL17 as a chemokine based on its predicted conformation. Recombinant CXCL17 was observed to dimerize as a function of concentration, a characteristic of several chemokines. Contrary to a previous report, CXCL17 was not chemotactic for murine splenocytes, although it was a low-potency chemoattractant for human neutrophils at micromolar concentrations, several orders of magnitude higher than those required for CXCL8. As anticipated owing to its highly basic nature, CXCL17 bound to GAGs robustly, with key C-terminal motifs implicated in this

process. While inactive via CXCR1, CXCL17 was found to inhibit CXCR1-mediated chemotaxis of transfectants to CXCL8 in a dose-dependent manner.

Discussion: In summary, despite finding little evidence for chemokine-like structure and function, CXCL17 readily bound GAGs, and could modulate chemotactic responses to another chemokine *in vitro*. We postulate that such modulation is a consequence of superior GAG binding, and that C-terminal fragments of CXCL17 may serve as prototypic inhibitors of chemokine function.

KEYWORDS

chemokine, chemotaxis, neutrophil, glycosaminoglycan (GAG), model, mucosal, CXCR1, CXCL8

1 Introduction

Chemokines are a family of approximately 40 small soluble cytokines in humans, noted for their chemoattractant properties, particularly for leukocytes (1). Despite quite varied degrees of homology, chemokines adopt the same characteristic "Greek-key" protein fold, consisting of three antiparallel β-strands overlaid by a C-terminal α-helix (2). The vast majority of chemokine family members fall into two classes known as CC and CXC chemokines, which describe the arrangement of conserved N-terminal cysteine residues that are either adjacent or interspersed with a single amino acid (3). As is the case with other leukocyte chemoattractants such as C5a and fMLP, chemokines exert their effects by binding to members of the G protein-coupled receptor (GPCR) superfamily expressed on the leukocyte surface (4–6).

CXCL17 was originally identified as a potential chemokine on the basis of apparent homology with CXCL8 as a result of molecular modeling efforts (7). However, the validity of this claim has recently been questioned by ourselves and others (8, 9). In a notable departure from most other chemokines, the primary structure of CXCL17 contains six conserved cysteine residues, a feature seen in only one other CXC chemokine, CXCL16 (10), and in the 6-Cys subset of CC chemokines composed of CCL1 (11), CCL15 (12), CCL21 (13), CCL23 (14), and CCL28 (15). CXCL17 is constitutively expressed at mucosal surfaces such as those in the proximal digestive tract, lung, and stomach (16, 17), although its precise function at these locations is not fully understood.

The mature CXCL17 protein sequence contains many arginine and lysine residues and, as a result, is predicted to be highly positively charged at a physiological pH with an isoelectric point (pI) of 10.95. This ranks it among the most cationic of CXC chemokines (18). This highly basic nature suggests that CXCL17 may play a role as an antimicrobial peptide, and *in vitro* data have been reported showing a broad spectrum of microbicidal activity against bacteria and fungi (16). Previous studies reported CXCL17 to be a chemoattractant for monocytes and dendritic cells (7, 17) and murine splenocytes (19). Deletion of the *cxcl17* gene in mice was observed to result in reduced numbers of alveolar macrophages within the lungs, which has led to suggestions of a role for CXCL17 in their recruitment (20). The GPCR known as GPR35 is expressed by some subsets of leukocytes and was postulated to be a receptor for CXCL17 (21), although this has been challenged by ourselves and others (22, 23). Notably, GPR35 was recently de-orphanized and identified as a receptor for the chemotactic serotonin metabolite, 5-hydroxyindoleacetic acid, which was shown to recruit GPR35$^+$ neutrophils at low nanomolar concentrations (24).

A currently unexplored possibility is that the high isoelectric point for CXCL17 may confer an ability to interact with extracellular matrix proteoglycans and glycosaminoglycans (GAGs) in the mucosae. GAGs are composed of heterogenous sub-populations of linear, highly sulfated polysaccharides, which, via covalent interactions with proteoglycans, reside in close association to cell membranes (25, 26). Chemokine–GAG interactions are widely reported elsewhere and are essential for retaining chemokine gradients on specific tissues and cell surfaces, while promoting and decoding chemokine signals that drive leukocyte motility, survival, and function [reviewed in (27, 28)]. However, the potential for GAG interactions with CXCL17 and their functional consequences are not yet known.

In this study, we report the chemotactic activity of CXCL17 for human neutrophils assessed using a real-time assay method, and the likelihood of CXCL17 adopting a chemokine-like fold using recent advances in molecular modeling. We also highlight the ability of CXCL17 to bind to GAGs and the effect of CXCL17 on the chemotactic responses of CXCR1 transfectants to CXCL8. Based on these findings, we suggest that CXCL17 may have modest chemotactic activity for neutrophils and that it can modulate the activity of other chemokines that depend on GAG binding for their activity.

2 Materials and methods

2.1 Materials

Materials were purchased from SIGMA-Aldrich (Poole, UK) unless otherwise stated. Oligonucleotide production and DNA sequencing services were from MWG-Biotech (Ebersberg,

Germany). HPLC materials were from Cytiva (Amersham, UK). Recombinant proteins and the small-molecule CXCR6 antagonist ML-339 were from R&D Systems (Bio-Techne Ltd., Abingdon, UK). Heparin dp8 and heparan sulfate (HS) used in the bio-layer interferometry (BLI) assays were from Iduron (Alderley Edge, UK). Primary antibodies used in Western blotting were sheep anti-human CXCL17 pAb (#AF4207), mouse anti-CXCL17 mAb (#MAB4207), and mouse anti-human CXCL4 mAb (#MAB7951) all from Bio-Techne. These were detected with either protein G-conjugated HRP or goat anti-mouse IgG Alexa Fluor Plus 800n, both from Thermofisher (Paisley, UK). All flow cytometry antibodies were purchased from BioLegend unless otherwise stated.

2.2 Signal peptide prediction, phylogenetic analysis, and prediction of glycosylation sites

Signal peptide cleavage prediction was performed on the full-length amino acid sequence for human CXCL17 (1–119) (Protein IUD Q6UXB2), using the Signal-P 6.0 server (29). CXCL17 was aligned against all other human CXC chemokines using SnapGene® software (Dotmatic, available at snapgene.com). Phylogenetic analysis was performed by EMBL-EBI MUSCLE alignment (30), with the results extracted and displayed as a midpoint rooted neighbor-joining tree without distance corrections using the interactive Tree Of Life (31). Secondary structure predictions were performed with the DSC server (32), showing predictions for CXCL8 (28–99) (P10145) and CXCL17 (24–119). Putative *N*-linked and *O*-linked glycosylation sites were predicted using the NetNGlyc-1.0 (33) and NetOGlyc-4.0 (34) servers, respectively.

2.3 *In silico* structural modeling of CXCL17

The CXCL17 (24–119) tertiary structure was predicted by AlphaFold2 (DeepMind, EMBL-EBI) using the ColabFold interface as described in (35). Target sequence was uploaded as a pdb70 template, and multiple sequence alignment (MSA) was performed by MMSeqs2 against Uniref and Environmental structure libraries with unpaired and paired sequences. Structural modeling was performed with AlphaFold2-ptm and AlphaFold multimer v2 predictions, with 3, 12, and 48 iterances of model recycling. A CXCL17 (24–119) homodimer structure was modeled using the same process with 12 iterances of model recycling. Stereochemical plausibility and confidence in the model were expressed in the predicted local distance test (plDDT) scores per residue (36), and by the Predicted Aligned Error (PAE) measured in Å distance (37). *De novo* folding of CXCL17 (24–119) was performed by specifying no template mode and single-sequence MSA mode for 48 model recycles. Predictions of the CXCL17 (24–119) structure by RoseTTAFold with ColabFold was performed by MMSeqs2 as described (35), and *de novo* folding was performed using single-sequence input. Predictions were run by RoseTTAFold for main-chain and Scrwl4 for side-chain predictions. Structural predictions generated by C-I-TASSER integrated the I-TASSER hierarchical structure modeling approach with deep learning-based contact predictions to guide Replica Exchange Monte Carlo (REMC) simulations to produce CXCL17 structure models as described (38).

2.4 Generation of CXCL4, CXCL17, and SUMO3-CXCL17 mutant constructs

The pE-SUMOpro3 AMP vector (Lifesensors Inc, PA, USA) was modified by site-directed mutagenesis to insert a silent *AgeI* restriction site in the final codon of the SUMO3 open reading frame (ORF). This facilitated subsequence cloning of chemokine inserts. The vector was renamed in-house as pEM-SUMOpro3 AMP. ORFs encoding the CXCL4 and CXCL17 (24–119) sequences without predicted signal peptides were subcloned into the pEM-SUMOpro3 AMP vector at the *AgeI* and *BamHI* sites. A panel of SUMO3-CXCL17 truncation mutants was generated by SDM by introducing stop codons at the required positions using the QuikChange II Site-Directed Mutagenesis Kit (Agilent Technologies; Santa Clara, USA).

2.5 Expression and purification of recombinant proteins

SUMO3-CXCL4 was expressed as inclusion bodies in BL21 (DE3) pLysS *E. coli*, as previously described (39). WT SUMO3-CXCL17 and variants were expressed as soluble proteins in SHuffle® T7 Competent *E. coli* (New England Biolabs, Hitchin, UK). In both protocols, protein was induced by the addition of 100 mM Isopropyl β-D-1-thiogalactopyranoside (IPTG) when cultures had reached log phase. Cultures were grown for a further 5 h after which pellets were harvested. Pellets were either stored at −20°C until further use or immediately lysed by sonication in HisTrap buffer A (50 mM Tris, pH 8.0, 150 mM NaCl, 10% glycerol, and 20 mM imidazole) supplemented with cOmplete™ Mini EDTA-free protease inhibitor cocktail. Lysates were clarified by centrifugation at 21,000 × *g* for 20 min followed by further clarification by 0.22 µm filtration.

Purifications were performed using an ÄKTA Pure Protein Purification System (Cytiva). CXCL4 was purified from inclusion bodies following solubilization in chaotropic buffer A (50 mM Tris, pH 8.0, 6 M GuHCl, 50 mM NaCl, and 20 mM imidazole) at room temperature (RT) overnight. Solubilized CXCL4 was loaded on a HisTrap HP 5-mL FF crude column and washed with 5 column volumes (CV) of chaotropic buffer A, and eluted with 0%–100% chaotropic buffer B (50 mM Tris pH 8.0, 6 M GuHCl, 50 mM NaCl, and 500 mM imidazole). The lysates containing SUMO3-CXCL17 and variants were loaded on a HisTrap HP 5-mL FF crude column pre-equilibrated with HisTrap buffer A. The column was washed with 20 CV of the same buffer, followed by a gradient of 0%–100% HisTrap Buffer B (50 mM Tris, pH 8.0, 150 mM NaCl, 10% glycerol, and 500 mM imidazole). Eluates were pooled and diluted to 0.5 mg/mL.

The SUMO3 tag was removed by digestion with a preparation of *Saccharomyces cerevisiae* Ubiquitin-like-specific protease 1

(*UlpI*), which was expressed in *E. coli* using a pET-28a construct and purified via an N-terminal 6xHis tag as previously described (40). For the SUMO3-CXCL4 construct, eluate was dialyzed into digestion buffer (50 mM Tris, pH 8.0, 150 mM NaCl, 10% glycerol, and 1 mM DTT) at 4˚C over 3 days. *UlpI* and SUMO3-CXCL4 were incubated at a 1:30 mass ratio at 4°C, with gentle stirring for 24 h. For CXCL17, *UlpI* and SUMO3-CXCL17 were incubated at a 1:25 mass ratio, in a non-reducing digestion buffer at 4°C for 24 h. Removal of the SUMO3-tag resulted in CXCL17 precipitating. The CXCL17 precipitate was subsequently solubilized in chaotropic buffer at RT for 24 h.

Separation of *UlpI* and the SUMO3 tag from free chemokine was performed on a HisTrap HP 1-mL column, pre-equilibrated with chaotropic buffer A supplemented with 1 mM DTT and CXCL17 eluted with chaotropic buffer A. Eluate was dialyzed into 50 mM Tris, pH 9.0, 150 mM NaCl, 10% glycerol, and 1 mM DTT at 4°C overnight. Purified CXCL4 and CXCL17 were refolded by "infinite" dilution (41) in cysteine/cystine, refolding buffer overnight at 4°C. Refolded CXCL4 and CXCL17 were purified on a HiTrap Heparin HP 1-mL column, washed with 20 CV HiTrap buffer A (50 mM Tris, pH 8.0, 150 mM NaCl, and 10% glycerol) and eluted with 10 CV 0%–100% gradient of HiTrap Buffer B (50 mM Tris, pH 8.0, 2.5 M NaCl, and 10% glycerol). Eluates were dialyzed into storage buffer (50 mM Tris, pH 8.0, 150 mM NaCl, and 10% glycerol) and snap frozen in liquid nitrogen for storage. The molecular mass and purity of CXCL4, CXCL17, SUMO3-CXCL17, and mutants were confirmed by SDS-PAGE, and identity was confirmed by Western blot. Concentration was assessed by human CXCL4 DuoSet ELISA (DY795) or SDS-PAGE followed by densitometry.

2.6 Cell culture and transfection

CHO-761H cells (42) were seeded in 24-well plates, at 2×10^5 cells/well in 24-Ham's F12 media, supplemented with glutamine, penicillin/streptomycin (PS), and 10% FBS. After resting for 24 h, cells were transfected with pmaxGFP (500 ng/μL) or pcDNA3.1-CXCL17 (194.1 ng/μL) using lipofectamine 3000 and were cultured in Opti-MEM media containing 1% PS. Mock-treated cells underwent the same transfection conditions in the absence of plasmid. After 48 h, cell supernatants (SN) were collected and cells were lysed in PBS, 1% IGEPAL, 0.4% iodoacetamide, 0.4% EDTA, and 2% protease inhibitors. pcDNA3.1-CXCL17 and mock SN was concentrated with 50 μL of HisPur™ Ni-NTA Resin (ThermoFisher). Transfected cells were analyzed by flow cytometry to confirm transfection efficacy and protein expression after 48 h. Cells were detached with Versene and resuspended in FACS buffer containing 1:10,000 TO-PRO-3 iodine, and samples were read with a FASCalibur flow cytometer (Becton Dickinson, UK), according to the manufacturer's instructions. To inhibit *O*-linked glycosylation, transfected CHO-761H cells were treated with 1–2 mM of Benzyl-GalNac (BGN) or DMSO vehicle control 1 h after transfection. Lysates were collected after 48 h and assessed by SDS-PAGE and Western blot.

Primary human neutrophils were isolated from healthy donor whole blood samples obtained with local ethical approval. Purification used the MACSxpress® Whole Blood Neutrophil Isolation Kit (Miltenyi) according to the manufacturer's instructions. Prior to chemotaxis assessment, neutrophils were resuspended to a concentration of 5×10^6 cells/mL in chemotaxis buffer RPMI-1640, 1% P/S, and 0.1% BSA and were rested for 1 h at 37°C. Murine IL-3-dependent pro-B-cells Ba/F3 were maintained in RPMI-1640, 10% FBS, 1% PS, and 50 μM 2-β-ME, supplemented with 1 ng/mL mouse IL-3 (Peprotech). The mouse pro-B cell L1.2 was maintained in identical media without the addition of IL-3. Stable hCXCR1 expressing Ba/F3 cells were generated by transfection in a 0.4-cm -electroporation cuvette with 50 μL of 10 mg/mL tRNA, with 1 μg of pcDNA3.1-CXCR1 plasmid at 330 V, 950 μF using a MicroPulser electroporator (Bio-Rad). Expression of CXCR1 was confirmed by flow cytometry as previously described (43), and maintained by antibiotic resistance selected by 1 mg/mL G418. Transiently transfected L1.2 cells were generated by transfection with a pcDNA3.1-CXCR6 plasmid by identical methodology. For both Ba/F3 and L1.2 cells, chemotactic responses were boosted by overnight culture with 10 mM sodium butyrate.

2.7 Isolation of mouse splenocytes

Eight- to 10-week-old female C57BL/6 mice were purchased from Charles River (Oxford, UK) and housed at Imperial College Central Biomedical Services facility. Mice were kept in specific pathogen-free conditions and provided autoclaved food, water, and bedding *ad libitum*. All animal procedures were performed in accordance with the recommendations in the Guide for the Use of Laboratory Animals of Imperial College London. All animal procedures and care conformed strictly to the UK Home Office Guidelines under the Animals (Scientific Procedures) Act 1986, and the protocols were approved by the Home Office of Great Britain.

2.8 Chemotaxis assays

Real-time chemotaxis assessment with the TAXIScan-12 system 2 (Hirata Corp., Japan) was performed as previously described (44). A total of 5×10^2 neutrophils were loaded onto the instrument in each channel, aligned, and then allowed to migrate for 60 min along chemokine gradients generated by the addition of 1 μL of recombinant 10 nM CXCL8 or varying concentrations of CXCL17 (24–119) purchased from R&D Systems. Basal migration was recorded in the absence of stimulus. Images were captured every 60 s and individual migration paths were manually tracked using the manual tracking function of ImageJ1.46. Chemotaxis was quantified using the IBIDI chemotaxis tool (45) and was expressed as directionality, velocity (μm/min), and *Y*-axis directional forward migration index (yFMI). yFMI describes the forward migration of cells parallel to the chemokine gradient and is calculated by dividing the Δy value of a cell track end-point by the total accumulated distance traveled.

Modified Boyden chamber assays were performed as previously described (23) using either 96-well CHEMO Tx® plates (Neuro Probe; Gaithersburg, MD) (43) for Ba/F3 and L1.2 transfectants or Corning® HTS Transwell®-96 plates for mouse splenocytes. Both systems had membranes with 5-μm pores. Dose responses to murine CXCL17 and CXCL12 were generated with C57BL/6 murine splenocytes seeded at 4×10^5 cells/well in 75-μL volumes. Dose responses to CXCL8 and CXCL17 were generated using Ba/F3 cells stably expressing CXCR1. Chemotaxis responses to human CXCL8, CXCL5, and CXCL6 either alone or in combination with CXCL17, and to CXCL8 alone or in combination with CXCL17, SUMO3-CXCL17, or SUMO3-CXCL17 Δ80 were generated using Ba/F3 cells stably expressing CXCR1. Dose responses to CXCL16 and CXCL17, and responses to CXCL16 alone or in combination with CXCL17 or ML-339 were generated using L1.2 cells transfected with CXCR6. In both systems, cells were suspended in chemotaxis buffer and allowed to migrate for 5 h at 37°C and 5% CO_2, after which cells traversing the membrane were enumerated by CellTiter-Glo® Luminescent Cell Viability Assay (Promega; Madison, WI) according to the manufacturer's protocol using a TopCount® NXT™ Microplate Scintillation and Luminescence Counter (Packard; Meriden, CT). The percentage of migrating cells was calculated as a percentage of the luminescence observed from cell inputs. Chemotactic indices were calculated by dividing the luminescence of cells migrating to stimulus by the basal level of migration.

2.9 Flow cytometry

Single-cell suspensions of total splenocytes pre-chemotaxis and following transmigration through the HTS Transwell®-96 pores in the absence or presence of stimuli were pelleted and washed in cold PBS. Cells were stained with the LIVE/DEAD Fixable Near IR Dead cell staining kit (Invitrogen) for 10 min at RT while shielded, and washed with flow cytometry buffer (PBS + 0.1% sodium azide + 1% BSA) and pelleted. Cells were then stained with rat anti-mouse CD45-BV711, rat anti-mouse CD3-PE-Cy7 (eBioscience), rat anti-mouse CD19-FITC, rat anti-mouse CD11b-Alexa Fluor 700, rat anti-mouse F4/80-PE, rat anti-mouse Gr-1-APC, and purified rat anti-mouse CD16/CD32 Fc Block™ (BD Biosciences) for 30 min at 4°C in flow cytometry buffer and then fixed in 1% paraformaldehyde. Sample acquisition was performed over 2 min per sample using a 5-laser BD LSR Fortessa III instrument (BD Biosciences), and all samples were kept as individuals and not pooled. Instrument standardization and calibration were performed according to the manufacturer's instructions. Compensation was accounted for using UltraComp eBeads™ (Thermo Fisher Scientific). Immune cell phenotyping was analyzed with FlowJo software (Version 10.9; BD Biosciences).

2.10 SDS-PAGE and Western blot

Proteins were resolved by reducing SDS-PAGE, using 12% NuPAGE Bis-Tris Mini Gels and MES buffer on a Mini Gel Tank (Invitrogen) according to the manufacturer's instructions. Proteins were transferred to nitrocellulose iBlot™ mini transfer stacks, with an iBlot™ gel transfer device and membranes were blocked with PBS containing 0.05% Tween-20 (PBS-T) and 5% (w/v) milk powder for 1 h and probed with 0.1 μg/mL of the relevant primary antibody in fresh blocking buffer overnight at 4°C with agitation. Blots were washed three times in PBS-T and probed with 0.2 μg/mL protein G-conjugated HRP or 0.1 μg/mL diluted goat anti-mouse IgG Alexa Fluor Plus 800 in blocking buffer at RT for 2 h with agitation. Blots were again washed three times in PBS-T and chemiluminescence was generated with Pierce ECL substrate and was imaged using an iBright™ instrument (ThermoFisher). Fluorescence was detected using an Odyssey XF imager (LI-COR, Cambridge UK).

2.11 Glycosaminoglycan solid-phase binding assays

Heparin from porcine intestinal mucosa (Merck), HS from bovine kidney (Merck), and chondroitin sulfate-A (CS) (Merck) were biotinylated as previously described in (46), using the EZ-Link Hydrazine-LC-Biotin kit (Thermofisher). Solid-phase binding assays were performed essentially as described previously (47). Recombinant proteins, either CXCL4, CXCL17 (24–119), SUMO3-CXCL17 (24–119), or SUMO3-CXCL17 truncation mutants, and SUMO3-tag were immobilized on 96-well EIA/RIA high binding plates (Corning) in coating buffer 20 mM Na_2CO_3, pH 9.6, overnight at RT. Wells were rinsed with 10 mM NaOAc, 150 mM NaCl, and 2% Tween-20, pH 6.0, and blocked with PBS and 5% BSA at 37°C for 90 min. Biotinylated heparin, HS, or CS was added at 1 μg/mL or as otherwise indicated, and bound for 4 h at RT. Plates were washed with PBS, and the bound GAG was probed by 1:400 streptavidin-HRP (R&D Systems), and subsequent incubation with TMB substrate (ThermoFisher) for 10 min. Reaction was stopped with 0.2 M H_2SO_4, and OD_{450nm} was measured with a SpectraMax i3x instrument (Molecular Devices). Background signals were corrected against blank wells, and data were analyzed and fit to non-linear hyperbola where X is concentration, to permit calculation of B_{max} and K_D values for GAG interaction with chemokine using Prism 9.2 (GraphPad, San Diego, CA).

2.12 Bio-layer interferometry to assess chemokine: GAG interactions

Real-time assessment of CXCL4 and CXCL17 binding to heparin dp8 and HS was assessed via BLI on an Octet Red96 system (Sartorius, Göttingen, Germany) using a methodology adapted from a previous study (48). Streptavidin-coated SAX biosensors (Sartorius) were hydrated for 10 min in assay buffer, 10 mM HEPES, pH 7.4, 150 mM NaCl, 3 mM EDTA, and 0.05% Tween-20, and coated with 0.078 μg/mL biotinylated heparin dp8 or 7.5 μg/mL biotinylated HS, until 0.5-nm and 0.15-nm wavelength shifts were detected, respectively. SAX sensors were washed in regeneration buffer, 0.1 M glycine, 2 M NaCl, and 0.1%

Tween-20, pH 9.5, and equilibrated in assay buffer. The Octet Red96 system performed a sensor check (2 0s), baseline reading (60 s), association phase (1,080 s), dissociation phase (1,500 s), regeneration (30 s, three times), and baseline reading (60 s), where reference and GAG-coated SAX sensors sampled 200-µL preparations of chemokine diluted in assay buffer. The binding signal data were recorded at 5 Hz and assessment of the dissociation off-rates of CXCL4 and CXCL17 binding to GAGs was performed in the Octet HT 10.0 analysis program. Curves were fitted to a dissociation phase with a 1:1 local model, and maximal responses (nm) and dissociation rate kDis (1/s) were calculated.

2.13 Statistical analyses

All statistical analyses were performed in Prism 9.2, using two-way ANOVA (unless indicated otherwise) with multiple comparisons and Dunnett's post-test. Statistically significant differences are displayed as $*p < 0.05$, $**p < 0.01$, $***p < 0.001$, and $****p < 0.0001$.

3 Results

3.1 *In silico* characterization of CXCL17 questions its classification as a chemokine based upon structural features

The CXCL17 gene in primates and rodents encodes a protein of 119 amino acids (7, 17, 49) with considerable homology between the human form ranging from 62.2% identity with the *Mus musculus* CXCL17 orthologue to 98.3% identity with the *Pan troglodytes* CXCL17 orthologue (9). After translation, an N-terminal signal peptide is cleaved from the full-length protein CXCL17 (1–119) to liberate mature CXCL17, although the first two publications to describe CXCL17 differ by one amino acid in their predicted cleavage sites (7, 49) despite using the same online prediction software. We used the latest version of SignalP6.0 to predict the likely mature form of CXCL17. The CXCL17 (23–119) species is predicted to be the mature form of human CXCL17 (97.76% likelihood) although the Leu24–Leu119 form of CXCL17 is the form commercially available. This form was used throughout this study unless indicated otherwise and is referred to as CXCL17 (24–119) (Figure 1A). Unique to CXCL17 among chemokines is the organization of the first four cysteines into two CXC motifs, with the first present within an extended N-terminus (Figure 1B). In agreement with a previous report (8), MSAs revealed low levels of primary sequence conservation to other CXC chemokines, with only 8.8%–18.3% identity. This contrasts with the relatively high levels of structural homology observed among the other CXC chemokines, where sequence identity is typically >30% (18), but ranges from 8.87% to 87.67% (data not shown). Subsequent phylogenetic analysis (Figure 1C) suggested that CXCL17 is, at best, a distant relative of the CXC chemokines with closest homology to CXCL16, another atypical CXC chemokine expressed as a type I membrane protein (10, 50). The structure of CXCL17 remains uncharacterized experimentally, although folding prediction with the DSC server predicts poor secondary structural homology to CXCL8 (Figure 1D). In contrast, the predicted secondary structure of CXCL8 (Figure 1D) is consistent with experimentally verified structures of the same chemokine (Figure 1E), containing the classical chemokine fold (51). The four cysteine residues of CXCL8 are correctly predicted to form disulfide linkages pairing Cys-7 with Cys-34 (C1–C3) and Cys-9 with Cys-50 (C2–C4) to stabilize the tertiary structure. In contrast, the secondary structure of CXCL17 is predicted to contain 4 α-helices with an absence of β-strands, inconsistent with the previous structural model generated by Pisabarro and colleagues (7), but supported and expanded upon by Denisov (8).

In the absence of structural data regarding CXCL17, we performed *in silico* modeling using ColabFold (35). The results of the highest ranking model generated with AlphaFold2 are shown in Figure 1F (and expanded upon in Supplementary Figure 1). Structural predictions of CXCL17 folding by AlphaFold2 ColabFold revealed little structural homology to CXCL8 or any other CXC chemokine. The C-terminal α-helix of CXCL17 is predicted to be exposed and is modeled with greater confidence than the rest of the molecule with plDDT residue scores above 70, and low PAE scores (Supplementary Figures 1H, I). Unlike the DSC secondary structure prediction, CXCL17 is not predicted to contain multiple α-helical regions, instead, the majority of the molecule is bundled into loose coiled formations with plDDT scores ranging from 40 to 65. A 90° rotation on the *Y*-axis reveals the N-terminus to be projected away from the core of the molecule. Disulfide bonding is predicted to take place in CXCL17, but contrasts with the C1–C3 and C2 C4 linkages observed in CXCL8 and other CXC chemokines. Disulfide bonds are predicted between Cys-50-Cys-110 (C1–C6) and Cys-77-Cys-103 (C4–C5). No linkage is predicted between Cys-52-Cys-75 (C2–C3), although their close proximity (modeled at 3.3 Å) suggests that a third pair of disulfide bonds within CXCL17 is a possibility. Additional structural modeling by C-I-TASSER partly corroborated the structural prediction made by AlphaFold2 ColabFold (Figure 1F), similarly predicting a C-terminal α-helical region, with the remainder of the protein composed of six short α-helices bundled into a compact conformation (Supplementary Figure 2). Modeling by RoseTTAFold using ColabFold MSA techniques predicted the presence of four α-helices but in an extended conformation, with the C-terminal helix corroborated by the other models also predicted with higher plDDT scores than the rest of the molecule (Supplementary Figures 3A–C). Because of the limitation of CXCL17 exhibiting low numbers of homologs in the Uniref90 and environmental databases searched on ColabFold, the predictions are of lower confidence than they would otherwise be for other better characterized sequences. To account for this, we also modeled CXCL17 (24–119) using *de novo* folding techniques within AlphaFold (Supplementary Figure 4) and RoseTTAFold (Supplementary Figures 3D–F) via ColabFold and again were unable to generate a predicated chemokine fold with both structures consisting of three to four α-helices interspersed with random coiled regions. In summary, using a complimentary series of modeling techniques, we were able to correctly model CXCL8

10.3389/fimmu.2023.1254697

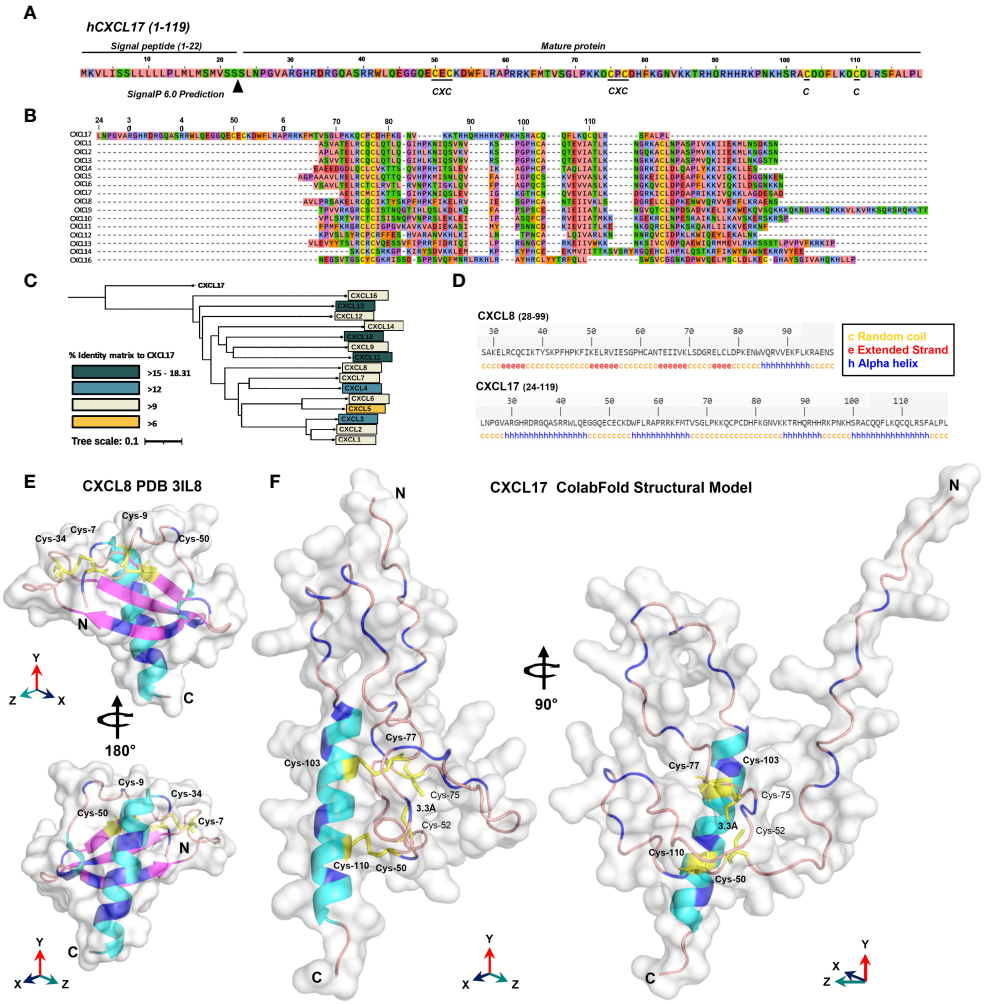

FIGURE 1
In silico analyses raise questions about the classification of CXCL17 as a chemokine. **(A)** The full-length amino acid sequence for human CXCL17 (1–119). The predicted signal peptide cleavage site and locations of CXC motifs and cystine residues are indicated. **(B)** MUSCLE multiple sequence alignment of all human CXC chemokine sequences, aligned against CXCL17 (24–119) using SnapGene. **(C)** Phylogenetic analysis of relationships between all human CXC chemokines. **(D)** DSC protein folding predictions for CXCL8 and CXCL17 (24–119). Regions are marked as random coil **(c)**, extended strand **(e)**, or alpha-helix **(a)**. **(E)** The solved structure of CXCL8. **(F)** Predicted structure of human CXCL17 (24–119) modeled by ColabFold with 48 recycles. E and F were generated in PyMOL with secondary structure indicated (α-helix, cyan; β-strand, magenta; random coil, salmon pink). The model is displayed with 90° or 180° *Y*-axis rotation; all cysteines are colored yellow and annotated, with those in disulfide bonds in bold. Arginine and lysine residues are colored blue.

from the primary sequence, but were unable to determine a chemokine fold for CXCL17 (24–119).

3.2 CXCL17 can form dimers and is not glycosylated post translation

A previous electrophoretic analysis of rat and human CXCL17 expressed by endogenous cells and transfectant cell lines suggested that full-length CXCL17 (1–119) undergoes proteolytic cleavage since two bands were observed by Western blotting: a larger pro-protein of a little over 20 kDa and a smaller protein running between 6 and 16 kDa (17). These forms were reported to represent CXCL17 (24–119) and CXCL17 (64–119) although the predicted molecular weights of these molecules (11.3 kDa and 6.6 kDa) do not tally precisely with those observed. We reassessed these findings by expressing the full-length ORF of human CXCL17 with a C-terminal His tag in CHO-L-761H cells. Cell lysates were generated and, following blotting, were probed with an anti-CXCL17 antiserum. CXCL17 was detected in transfected cells but not in mock-transfected cells running under reducing conditions with estimated molecular weights of approximately 15 and 30 kDa (Figure 2A). Under the same conditions, commercially available human CXCL17 (24–119), which was produced in *E. coli*, ran with slightly lower molecular weights of 14 kDa and 28 kDa, resembling the two bands previously reported by Lee and co-workers (17). Since the recombinant CXCL17 (24–119) had not been exposed to eukaryotic signal peptide cleavage proteases, we hypothesized that these bands represented monomers and dimers of the CXCL17 (24–119) species. Since a property of chemokines is to form dimers and

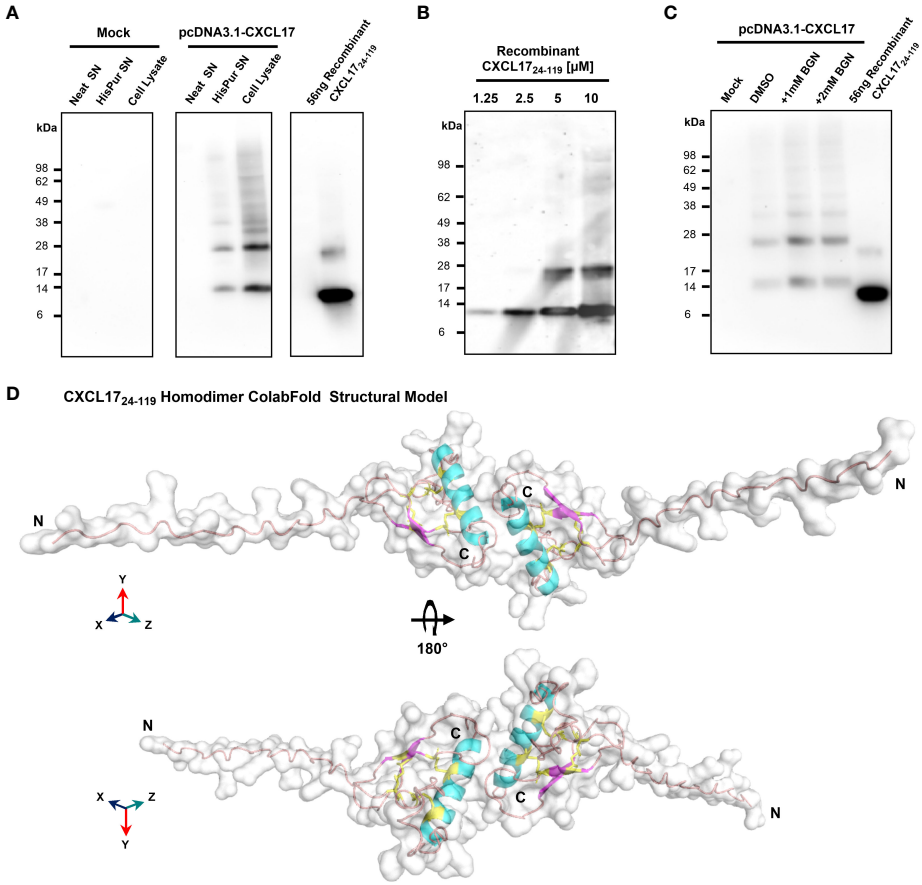

FIGURE 2
CXCL17 assembles into multimers and is not glycosylated. **(A)** Western blotting of concentrated CHO-761H supernatants following either mock transfection or transfection with pCDNA3.1 containing a C-terminally His-tagged CXCL17 ORF. Recombinant CXCL17 (24–119) was analyzed alongside as a control. Data are representative of three experiments. **(B)** Western blotting of serial dilutions of bacterially expressed recombinant CXCL17 (24–119). **(C)** *O*-linked glycosylation of CXCL17 in CHO-761H cells was inhibited by culture with the indicated concentrations of Benzyl-GalNac (BGN) or vehicle control (DMSO). All Western blots are representative of three independent experiments. **(D)** ColabFold structural model of a CXCL17 (24–119) homodimer. Models were generated in PyMOL with molecular surface and secondary structures indicated. The model is rotated 180° in the *X*-axis, with cysteines colored yellow and represented as sticks. N- and C-termini are annotated with N and C, respectively.

higher-order oligomers as a function of increased concentration (48), we assessed the apparent molecular weights of recombinant CXCL17 (24–119) in the 1.25–10 μM range via Western blot (Figure 2B). At a concentration of 5 μM and above, CXCL17 was observed to form the 28-kDa species in an apparent 3:1 ratio of monomer:dimer, respectively.

Since glycosylation can also influence the apparent molecular weight of proteins, the NetOGlyc-4.0 and NetNGlyc-1.0 servers were used to predict putative glycosylation sites. Seven potential *O*-glycosylation sites but no *N*-linked sites were predicted within the CXCL17 primary sequence. CHO-L-761H cells were transfected with the CXCL17 (1–119) his-tagged construct and *O*-linked glycosylation was inhibited by supplementing cultures with benzyl-2-acetamido-2-deoxy-a-D-galactapyranoside (BGN). Inhibition of *O*-linked glycosylation by BGN revealed no change in apparent molecular mass, suggesting that CXCL17 does not undergo post-translational glycosylation (Figure 2C).

Since CXCL17 appears to form dimers, a model of CXCL17 (24–119) dimer formation was generated in AlphaFold2 ColabFold (Figure 2D; expanded details in Supplementary Figure 5). The model predicted that CXCL17 dimerizes along an interface containing their respective exposed C-terminal α-helices, oriented end-to-end. The dimer model has a different pattern of disulfide bond formation than the monomer, with 3-disulfide bonds predicted to form between Cys77–103 (C4–C5), Cys52–110 (C2–C6), and Cys50–75 (C1–C3). Interestingly, the model also predicts that structural changes take place within each of the constitutive monomers, with the formation of a short region of two antiparallel β-strands, and an extended N-terminus that is projected into space away from the dimer complex.

3.3 CXCL17 (24–119) fails to recruit murine splenocytes

CXCL17 has previously been reported to be chemotactic for dendritic cells and monocytes (7), although we and others have struggled to show robust chemotactic activity for monocytes and

THP-1 cells using commercially available CXCL17 (24–119) (22, 23). In modified Boyden chamber assays, recombinant mouse CXCL17 (23–119) was previously reported to attract a subpopulation of splenocytes ($CD11b^{+}Gr\text{-}1^{high}$ $F4/80^{-}$ cells) isolated from SCID mice in a dose-dependent, pertussis toxin-sensitive manner (19). We re-assessed these studies using splenocytes isolated from C57BL/6 mice and a broad concentration range of mouse CXCL17 (23–119) with 100 nM CXCL12 as a positive control. Flow cytometric analysis of the splenocytes showed the $CD45^{+}$ population to be predominantly composed of T cells and B cells, with low percentages of neutrophils and monocytes/macrophages (Figure 3A). In Boyden chamber chemotaxis assays, mouse splenocytes responded robustly to CXCL12, which was statistically significant when compared with basal migration (Figure 3B). In contrast, exposure of the same splenocytes to a broad concentration range of mouse CXCL17 (23–119) failed to elicit significant levels of chemotaxis and, at the highest concentration of 5 μM CXCL17 (23–119), resulted in migration at levels significantly lower than those observed in the absence of a stimulus. To further dissect these data, we carried out flow cytometry on a proportion of the cells recovered from the Boyden chamber after chemotaxis (Figures 3C–H). Although CXCL12 was seen to recruit T cells, B cells, neutrophils, and monocytes/macrophages with varying efficacy, these leukocyte subsets were unresponsive to all CXCL17 concentrations examined. Notably, we found that the CD11b+GR-1hi $F4/80^{-}$ fraction of splenocytes reported by Matsui et al., to respond to CXCL17, were unresponsive in our assays (Figures 3G, H). We therefore conclude that mouse CXCL17 (23–119) is not a major chemoattractant for mouse splenocytes.

3.4 CXCL17 is a weak chemoattractant for human neutrophils

To date, no reports of CXCL17 having chemotactic activity for human neutrophils have been described. We therefore investigated the potential for human CXCL17 to recruit freshly isolated human neutrophils, using a real-time chemotaxis assay (TAXIScan) (52). In this system, a chemoattractant gradient is formed by the addition of 1 μL of varying concentrations of chemoattractant and the migration of individual cells is tracked microscopically as a function of time. A CXCL8 gradient was used as a positive control. Human neutrophils exposed to a gradient formed by 1 μL of 10 nM CXCL8 responded with robust chemotaxis when compared to neutrophils analyzed in the absence of a chemoattractant (Figures 4A, B). In contrast, responses to a range of CXCL17 (24–119) gradients revealed little in the way of chemotactic activity until 1 μL of 5 μM CXCL17 was employed (Figures 4C–F). Analysis of the individual tracks of neutrophils allowed the determination of the velocity, directionality, and yFMI parameters (Figures 4G–I). In agreement with the cell tracks, only the parameters of chemotactic responses to 10 nM CXCL8 and 5 μM CXCL17 were found to be significantly different from those determined in the absence of a chemoattractant. Thus, we conclude that CXCL17 (24–119) had modest chemotactic activity for human neutrophils.

3.5 Solid-phase assays reveal CXCL17 binds glycosaminoglycans with greater capacity than CXCL4

A key requirement for the chemotactic function of many chemokines *in vivo* is the ability to bind to GAGs on the surface of cells (53). Given the relatively high isoelectric point of CXCL17, we tested the hypothesis that CXCL17 would bind to GAGs using a solid-phase binding assay (54). CXCL4, originally identified due to its heparin binding properties (55), and subsequently characterized as having a low nM affinity for binding heparin, HS, and chondroitin sulfate (CS) (48), was used as a positive control (Figures 5A–C). A broad concentration range of immobilized CXCL17 was seen to bind heparin, HS, and CS with a significantly greater capacity than equimolar concentrations of CXCL4, as determined by the percentage of maximal binding, which, in all cases, was to either 500 nM or 1 μM CXCL17 coatings. The maximal recovered binding signal of all three GAGs tested was consistently higher when bound to CXCL17 than for CXCL4, indicating that immobilized CXCL17 exhibited a greater capacity for binding GAGs than CXCL4 in this assay. However, care must be taken when interpreting this observation as immobilization of the chemokine may disrupt typical oligomerization dynamics that occur when binding to GAGs, and the proteins may have varying adsorption rates to polystyrene plastics, which could impact the absolute amount of immobilized chemokine present in this assay.

To directly compare the affinity of binding associations of heparin, HS, and CS to CXCL17, a fixed concentration of CXCL17 was immobilized, and varying concentrations of GAG were bound (Figure 5D). Curve fit analysis (Table 1) revealed that the calculated K_D values for GAG binding to CXCL17 were in the mid-low nanomolar range. The recovered binding signal was normalized to the maximal signal from the experiment (1,000 ng/mL HS), which permitted relative comparison between the overall levels of CXCL17 binding capacity for the different GAGs. Immobilized CXCL17 exhibited the greatest capacity for binding HS, and while the binding of the maximum concentration of CS exceeded that of heparin, curve fit analysis revealed that the B_{max} value of heparin was higher than CS, indicating that CXCL17 may have a lower affinity, but higher binding capacity for heparin than CS.

We also assessed the extent to which the CXCL4 and CXCL17 tertiary structure contributes to the GAG-binding activity by reducing intermolecular disulfide bonds within CXCL17 and CXCL4. These proteins were then immobilized and chemokine binding to heparin, HS, and CS was assessed (Figures 5E–G). Reduction significantly reduced the binding of all three GAGs to CXCL4, but had negligible impact on GAG binding to CXCL17, suggesting that the interactions of CXCL4 and CXCL17 with GAGs have different structural requirements.

10.3389/fimmu.2023.1254697

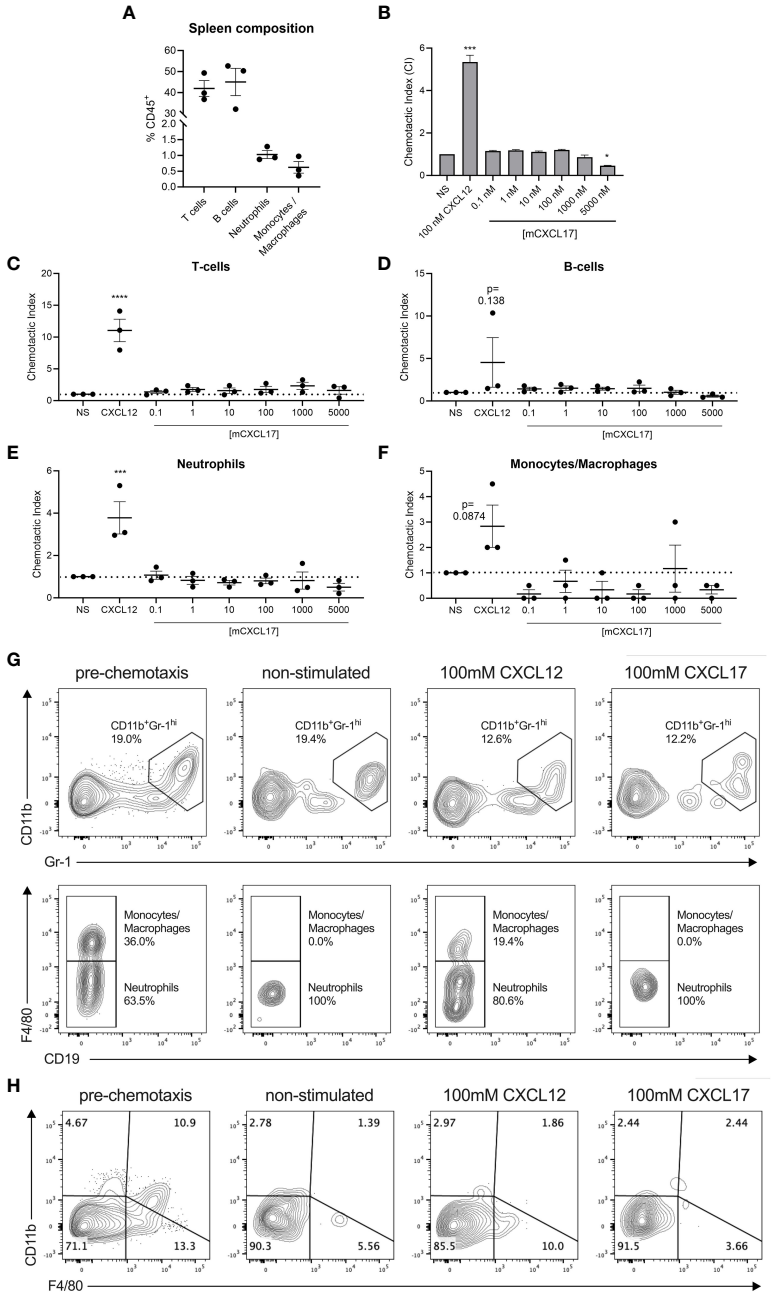

FIGURE 3
CXCL17 does not induce chemotaxis of murine splenocytes. **(A)** The phenotypic composition of total C57BL/6 murine splenocyte populations prior to the assessment of chemotaxis was characterized by flow cytometry after cell debris, doublets, and non-viable and CD45- cells were excluded. CD45+ leukocytes were gated into CD3+CD19- T cell, CD3-CD19+ B cell, CD3-CD19-CD11b+Gr-1hiF4/80- neutrophil, and CD3-CD19-CD11b+Gr-1hiF4/80+ monocyte/macrophage populations, and are presented as % of the total events within the CD45+ cell compartment. **(B)** Transwell assay showing the chemotactic index of total splenocytes responding to recombinant CXCL12 or mCXCL17 (23–119), assessed by CellTiter-Glo® luminescence assay (n = 3). **(C–F)** Transmigrating cells were characterized by flow cytometry in the absence or presence of CXCL12 or mCXCL17 (23–119), to identify changes in the proportions of recruited **(C)** T cells, **(D)** B cells, **(E)** neutrophils, and **(F)** monocytes/macrophages. Samples were normalized by assessing equal volumes of the transmigrated cell suspension, and counting the total number of cell events in a 2-min acquisition period as a fold change from non-stimulated (NS) cells. Data are presented as chemotactic index, from three independent experiments. Data are displayed as mean ± SEM, and two-way ANOVA with Sidak's multiple comparisons was performed and statistical significance is displayed as *p < 0.05, ***p < 0.001, and ****p < 0.0001. **(G, H)** Representative flow cytometry plots illustrating the distribution of events from a 2-min acquisition of equal volumes of splenocytes pre-chemotaxis, or following transmigration in the absence or presence of 100 nM CXCL12 or 100 nM mCXCL17 (23–119). Data were pre-gated on CD45+CD3-CD19- cells and show the distribution along **(G)** CD11b and Gr-1 axes (top panel), and subsequent gating within the CD11b+Gr-1hi population for F4/80 expression (bottom panel). **(H)** Representative flow cytometry plots pre-gated on CD45+ only, displaying the phenotypic distribution along CD11b and F4/80 axes. Plots show data from one experiment, which was representative of three independent experiments.

10.3389/fimmu.2023.1254697

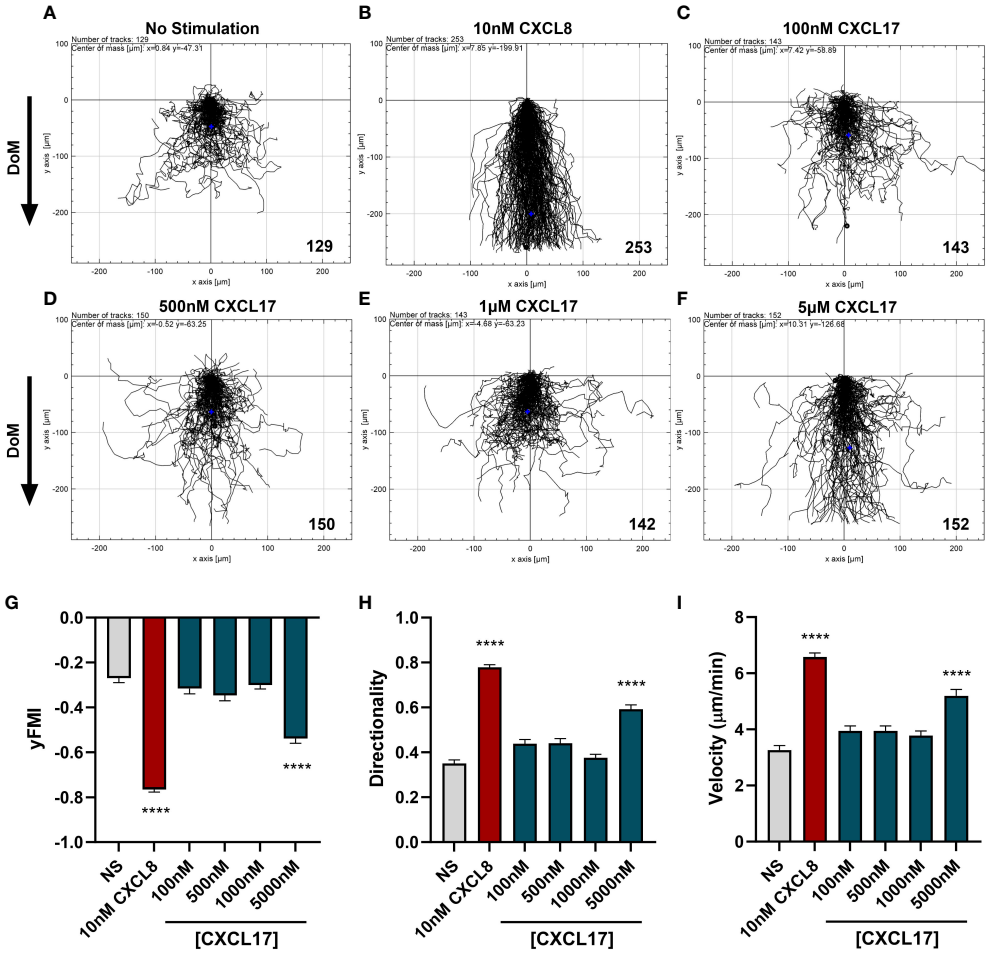

FIGURE 4
CXCL17 is a comparatively weak chemoattractant for neutrophils. Migration of individual neutrophils was assessed using the EZ TAXIScan real-time chemotaxis assay, in the absence of stimulus **(A)**, and after addition of various concentrations of CXCL8 **(B)**, or CXCL17 (24–119) **(C–F)**. Direction of movement (DoM) is indicated by an arrow. Individual paths were collated, with the total number of cells tracked at each condition indicated in the bottom right of the respective *XY*-plots. Aggregated chemotaxis from eight independent donors was analyzed and pooled to calculate *Y*-axis forward migration index (yFMI) **(G)**, directionality **(H)**, and velocity **(I)** of responses. Data are displayed as mean + SEM, and all statistical analyses were made as comparisons against the no-stimulus control. One-way ANOVA with a Dunnett's Multiple Comparison test was performed on biological replicates (n = 8) and statistical significance is displayed as ****$p < 0.0001$.

3.6 Bio-layer interferometry reveals that CXCL17 and CXCL4 have comparable dissociation rates when binding heparin and heparan sulfate

The GAG binding interactions of CXCL17 and CXCL4 were further investigated by BLI (56, 57). In this assay, the dynamic binding interactions between sensors coated with biotinylated heparin dp8 or HS and soluble chemokine analyte were quantified by optical wavelength shift during association and dissociation stages of binding. Heparin demonstrated comparable binding capacities for CXCL4 and CXCL17 at analyte concentrations above 62.5 nM, but displayed a greater capacity for binding CXCL17 compared to CXCL4 at concentrations below this (Figure 6A). In contrast, HS exhibited comparable binding capacities for CXCL4 and CXCL17 at all concentrations tested (Figure 6B). The binding of 250 nM CXCL17 to heparin and HS was characterized by a biphasic association curve for which a global, 1:1 model "Global full" could not be confidently applied, where for the first 100 s of interaction, the rate of association was rapid then decelerated until ~250 s where it reached its maximal association (Figures 6A, B). Such deviations from pseudo-first order binding are typically observed as a feature of mass transport limitation (MTL), or may instead be explained due to surface ligand heterogeneity and the presence of multivalent attachment sites for the analyte due to oligomer formation (58, 59). MTL effects occur more frequently when binding to dense heterogenous ligands like GAGs, which influence local analyte diffusion to and from the bulk, but here we know that both CXCL17 and CXCL4, exhibiting multimer forming capabilities, may simultaneously interact with the surface via multiple interaction sites. This biphasic association was only apparent when 250 nM CXCL17 was used and may suggest differing affinities of interaction for CXCL17 with GAGs, and between CXCL17 monomers during multimer assembly. When CXCL17 was diluted to 62.5 nM or below, the biphasic curve of binding to heparin and HS was lost, perhaps since the rate of

10.3389/fimmu.2023.1254697

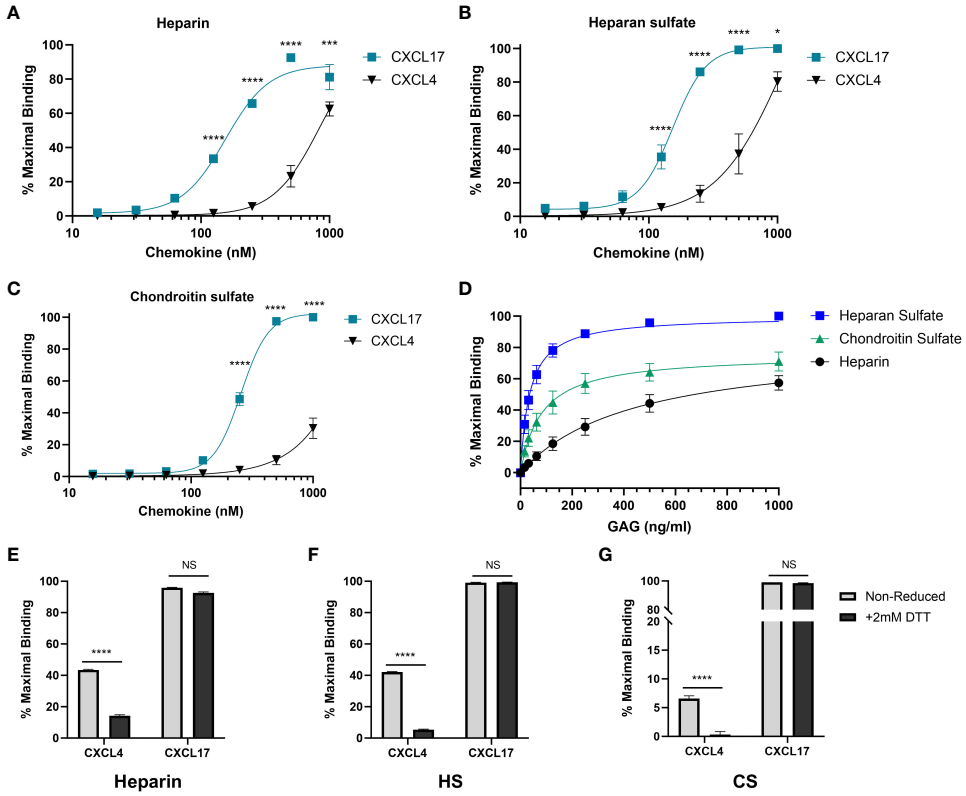

FIGURE 5
CXCL17 is an efficacious binder of glycosaminoglycans. **(A–C)** The binding of heparin **(A)**, HS **(B)**, or CS **(C)** by immobilized recombinant CXCL17 (24–119) or CXCL4 (n = 4). **(D)** CXCL17 (24–119) (500 nM) was immobilized, and binding of increasing concentrations of biotinylated heparin, HS, and CS was assessed (n = 3). **(E–G)** Chemokines were immobilized in both their native state and following reduction with 2 mM DTT, after which the binding of 1 µg/mL heparin, HS, or CS was quantified (n = 3). In all cases, data were normalized to the maximum binding signal recorded for the experiment, with data presented as a percentage of this signal and displayed as mean ± SEM. Two-way ANOVA with Fisher's LSD post-test [for **(A–C)**], or Sidak's multiple comparison test [for **(E–F)**] was performed. Statistical significance is displayed as *p < 0.05, ***p < 0.001, ****p < 0.0001. NS refers to no stimulus.

CXCL17 dimer formation was diminished at lower concentrations of chemokine. For CXCL4, no biphasic curves were observed, which suggests that CXCL4 binds heparin and HS with approximately the same affinity with which it forms multimers, with both events occurring at physiologically relevant concentrations of chemokine.

Owing to the inability to fit a global, 1:1 model, we opted to compare the dissociation curves for CXCL4 and CXCL17 for which high-quality local curve fits could be applied, and for which previous studies have demonstrated a relationship between slow rates of dissociation and high binding affinity for CXCL4 (60). The dissociation rates for CXCL4 and CXCL17 from both GAGs were highly comparable at equimolar concentrations (Table 2). For CXCL4 vs. HS or heparin, and for CXCL17 vs. heparin, the dissociation rates decreased alongside the analyte concentration. Such an observation is characteristic of MTL, but may also occur when a sub-population of analyte oligomers is bound simultaneously to the surface via multiple interaction sites, with this sub-population exhibiting slower dissociation kinetics since

TABLE 1 The maximal binding and K_D of heparin, heparan sulfate, and chondroitin sulfate to immobilized CXCL17 (24–119).

GAG	Average molecular mass (g mol^{-1})	B_{max} (% Maximal binding)	Equilibrium dissociation constant (ng/mL)	K_D (nM)	R^2
Heparin	6,000	82.51	439.50	73.25	0.9997
Heparan sulfate	30,000	103.10	38.79	1.29	0.9996
Chondroitin sulfate	21,000	75.52	81.39	3.88	0.9985

Binding associations of heparin, HS, and CS to immobilized recombinant CXCL17 (24–119) were calculated using a solid-phase binding assay (Figure 4D). CXCL17 (500 nM) was immobilized, to which 1,000, 500, 250, 125, 62.5, 31.25, 15.625, and 0 ng/mL heparin, HS, or CS were bound and quantified at OD_{450nm} by a colorimetric assay (n = 3). Curves were fit using GraphPad Prism non-linear fit analysis, and display hyperbola where X is concentration. Best-fit values to the mean data points of three independent experiments were calculated for B_{max} and K_D of each GAG binding to immobilized CXCL17 (24–119). The goodness of fit is displayed by the R^2 values.

10.3389/fimmu.2023.1254697

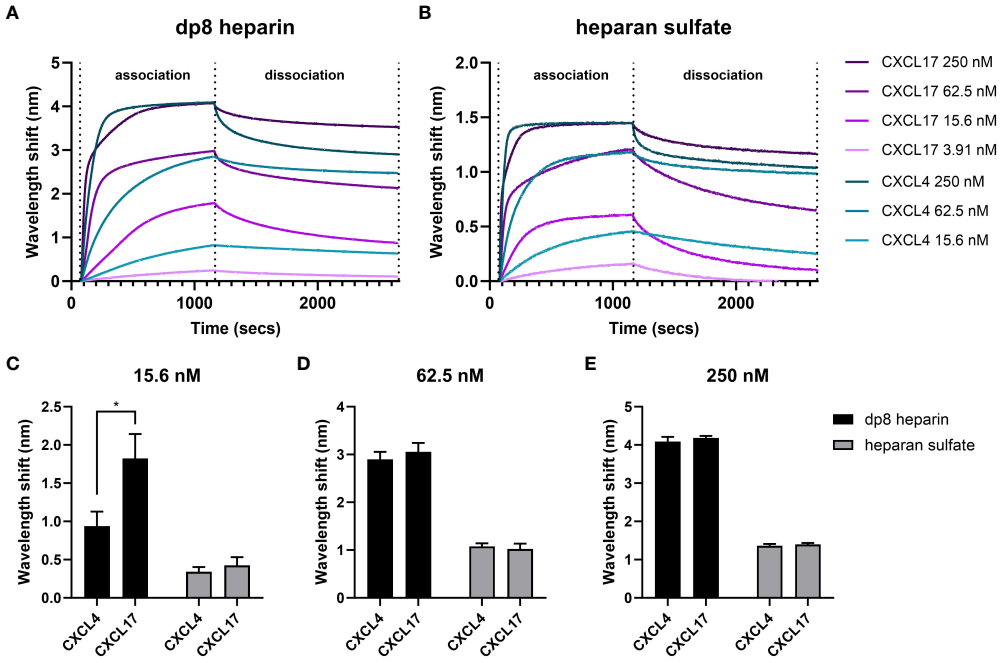

FIGURE 6
CXCL4 and CXCL17 bind heparin and heparan sulfate with high capacities. Real-time assessment of CXCL4 and CXCL17 (24–119) binding to immobilized heparin (dp8) and HS as assessed by bio-layer interferometry (BLI). Sensorgrams illustrate the binding associations between streptavidin immobilized biotinylated heparin **(A)**, or HS **(B)**, and various equimolar concentrations of CXCL4 and CXCL17. Prepared solutions of chemokine were sampled with BLI (Octet) streptavidin-coated sensors containing bound GAG, for a 1,080-s association phase, and a 1,500-s dissociation phase. The experiment was performed in triplicate with data displayed as wavelength shift (nm) from a single representative sensorgram plot. **(C–E)** The extent of molecular association of CXCL4 or CXCL17 with heparin or HS at increasing concentrations of chemokine. Measurements were taken of induced wavelength shift (nm), with maximal recorded wavelength shifts for 15.6 nM **(C)**, 62.5 nM **(D)**, and 250 nM **(E)** of chemokine. Data are displayed as mean wavelength shift (nm) + SEM from three independent experiments, and two-way ANOVA with Sidak's multiple comparison test was performed, and statistical significance is displayed as $*p < 0.05$.

both attachments must be broken simultaneously to permit free dissociation (58). Conversely, the dissociation rate for CXCL17 binding to HS was not dose dependent in the same manner and would therefore not support these curve deviations being MTL mediated. Together, these findings suggest that when chemokine concentration is highest, the rate of dissociation from the GAGs is fastest. We may speculate that this is partly driven by chemokine dissociation from clustered multimer complexes on the bound GAG, where the affinity for binding the multimer complex is lower than the affinity for binding GAG. Together, these observations suggest that concentration-dependent CXCL17 multimers may play a role in mediating dynamic GAG interactions.

Additionally, it was observed that higher concentrations of CXCL17 failed to completely dissociate from the immobilized heparin or HS during the wash step performed between experimental replicates (Figures 6A, B). This observation further

TABLE 2 CXCL4 and CXCL17 bind GAGs with high capacity and with comparable dissociation rates.

Chemokine	Conc. (nM)	Maximum Response (nm)		kDis (1/s) $\times 10^{-3}$		Dissoc. X^2		Dissoc. R^2	
		HP	HS	HP	HS	HP	HS	HP	HS
CXCL4	**250**	4.091	1.359	2.225	1.530	0.571	0.089	0.996	0.995
	62.5	2.897	1.079	1.404	1.421	0.097	0.050	0.998	0.995
	15.625	0.938	0.340	0.326	0.540	0.013	0.023	0.999	0.997
CXCL17	**250**	4.180	1.398	2.129	1.454	0.115	0.053	0.997	0.997
	62.5	3.056	1.023	1.241	1.205	0.363	0.051	0.998	0.999
	15.625	1.824	0.424	1.407	2.132	0.234	0.050	0.999	0.997
	3.906	0.315	0.077	1.029	2.471	0.021	0.023	0.997	0.952

The dissociation rates (kDis) of CXCL4 and CXCL17, from heparin (dp8) and HS, were calculated using curve fit analysis software from Octet (Sartorius). Local individual curve fits were performed to the dissociation phase of the BLI sensorgrams using a fast 1:1 local model and were used to calculate the kDis (1/s). The quality of the data fitting is reflected by the X^2 value, and the goodness of fit is expressed by the R^2 value. Data display mean values calculated from individual curve fits, from three independent experiments.

10.3389/fimmu.2023.1254697

supports the notion of multivalent binding between CXCL17 and immobilized GAGs, and therefore necessitated the preparation of fresh GAG-coated biosensors between experimental replicates.

The total extent of chemokine–GAG binding associations was estimated by the amount of optical wavelength shift (nm) on the BLI sensor surface, which is proportional to the amount of analyte mass bound to the GAG-coated sensor. Taking different concentrations of CXCL4 and CXCL17 (15.6, 62.5, and 250 nM) and comparing the maximal wavelength shift at the association phase end-point, the relative amount of chemokine accumulation on the GAG was inferred (Figures 6C–E). In contrast with our solid-phase binding assays (Figure 5), we observed that on HS, the total binding capacity for CXCL4 and CXCL17 was approximately equal at all analyte concentrations tested (Figures 6C–E). On heparin, both CXCL4 and CXCL17 accumulated to comparable levels at concentrations above 62.5 nM (Figures 6D, E), but when the analytes were diluted to 15.6 nM, heparin bound a significantly greater mass of CXCL17 compared to CXCL4 (Figure 6C), suggesting that in this assay with immobilized GAGs, heparin has a higher capacity for binding low concentrations of CXCL17 than CXCL4.

All in all, the BLI assays determined that under dynamic conditions containing free chemokine and immobilized GAG, CXCL17 and CXCL4 demonstrated comparable levels of accumulation on heparin and HS, while CXCL17 exhibited selectively greater accumulation on heparin at the lowest concentrations tested.

3.7 Truncation of CXCL17 identifies GAG binding motifs within the C-terminus

GAG binding motifs encoded within the primary structures of several chemokines have been studied by several groups and typically rely on the juxtaposition of amino acids with basic side chains such as lysine and arginine. This is exemplified by the BBXB and BBBXXB motifs where B represents a basic amino acid (61). Analysis of the CXCL17 (24–119) sequence revealed several putative GAG binding motifs as highlighted in Figure 7A. We therefore carried out a program of mutagenesis to identify residues involved in GAG binding. Four truncation mutants (Δ20, Δ40, Δ60, and Δ80) were generated in which the C-terminus of CXCL17 was progressively truncated by 20 amino acids.

Proteins were expressed as N-terminal fusions with the partner protein SUMO3, which we and others have previously used to improve the stability and yield of recombinant chemokine (40, 41). Typically, in this system, the SUMO3 portion is removed post expression via enzymatic cleavage with *UlpI* to yield the mature protein (Supplementary Figure 6). However, given that some truncation mutants were short and difficult to resolve via SDS-PAGE, we opted to retain the N-terminal SUMO3 fusion partner having first shown that SUMO3 does not bind to GAGs, nor does it grossly interfere with the ability of SUMO3-CXCL17 to bind to GAGs (Supplementary Figure 7). Constructs encoding SUMO3-CXCL17 (24–119) and the CXCL17 truncation mutants were expressed and purified to homogeneity (Figure 7B). Subsequently,

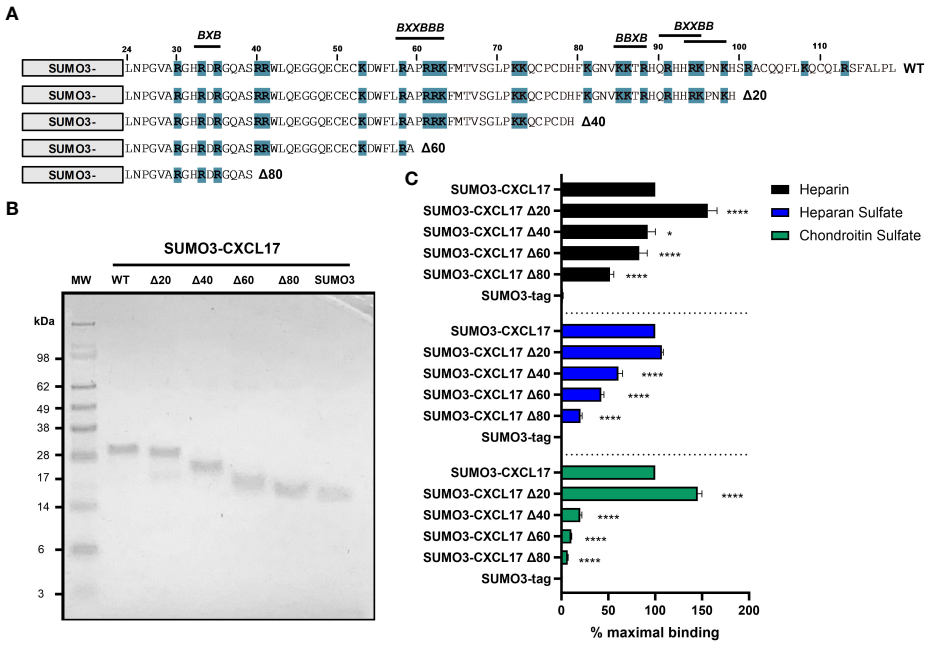

FIGURE 7
The extreme C-terminus of CXCL17 occludes a cryptic GAG-binding domain. **(A)** Schematic representation of C-terminal truncations of SUMO3-CXCL17 (24–119) generated. Lysine and arginine residues are highlighted blue and putative GAG binding regions are indicated, where B denotes a basic residue and X denotes any residue. **(B)** Recombinant SUMO3-CXCL17 truncations as resolved by reducing SDS-PAGE. **(C)** Binding interactions of GAGs to immobilized SUMO3-CXCL17 truncation mutants as assessed using a solid-phase binding assay. Chemokines were immobilized and the binding of heparin, HS, and CS was quantified, with the % maximal binding normalized to that of the full-length SUMO3-CXCL17 (24–119). Data are displayed as mean + SEM (n = 4) and two-way ANOVA with Dunnett's multiple comparison test was performed. Statistical significance is displayed as *p < 0.05, ****p < 0.0001.

they were assessed for their ability to bind a fixed concentration of heparin, HS, or CS using a solid-phase GAG-binding assay (Figure 7C). Binding to all three GAGs was improved by removal of the first 20 C-terminal residues (Δ20 construct). Specifically, binding of the Δ20 construct to heparin and CS, significantly increased to more than 140% of that observed with the parent SUMO3-CXCL17 (24–119). Removal of a further 20 residues (Δ40 construct) resulted in significant decreases in binding to all three GAGs when compared with SUMO3-CXCL17 (24–119) with the greatest reduction observed in the binding of CS. Consecutive deletion of a further 20 amino acids (Δ60 and Δ80 constructs) reduced the binding of all three GAGs, with heparin binding the most resilient to truncation, retaining approximately 45% of the heparin binding capacity of SUMO3-CXCL17 (24–119) even when 80 C-terminal residues had been removed.

3.8 CXCL17 inhibits CXCL8-mediated chemotaxis of CXCR1-Ba/F3 transfectants

Interactions with GAGs on the neutrophil cell surface are essential for responses to the chemokine CXCL8 as highlighted by the pathogen *Streptococcus pyogenes*. Invasive strains of this bacterium produce an enzyme known as SpyCEP, which cleaves the major GAG binding domain from CXCL8, rendering the chemokine impotent (44). We therefore postulated that CXCL17 may be able to inhibit chemotactic responses to CXCL8 by disrupting GAG binding. In modified Boyden chamber assays using a Ba/F3 cell line expressing CXCR1, a robust characteristic bell-shaped dose response to CXCL8 was observed with CXCL17 inactive over the same concentration range (Figure 8A). No chemotaxis of parental Ba/F3 cells in response to a range of CXCL8 or CXCL17 concentrations was detected (data not shown). Employing a sub-optimal concentration of CXCL8 (0.1 nM) in the presence or absence of increasing concentrations of CXCL17, we found that concentrations of CXCL17 between 1 nM and 1 μM significantly inhibited chemotactic responses to CXCL8, with the uppermost CXCL17 concentration reducing migration to basal levels (Figure 8B). This inhibition was also observed for two other CXCR1 ligands, CXCL5 and CXCL6, suggesting a broad range of inhibition (Figure 8C). Since CXCL16 is the CXC chemokine with nearest homology to CXCL17, we also assessed agonist and antagonist activity at CXCR6. Although robust responses of CXCR6 transfectants were observed to CXCL16, no

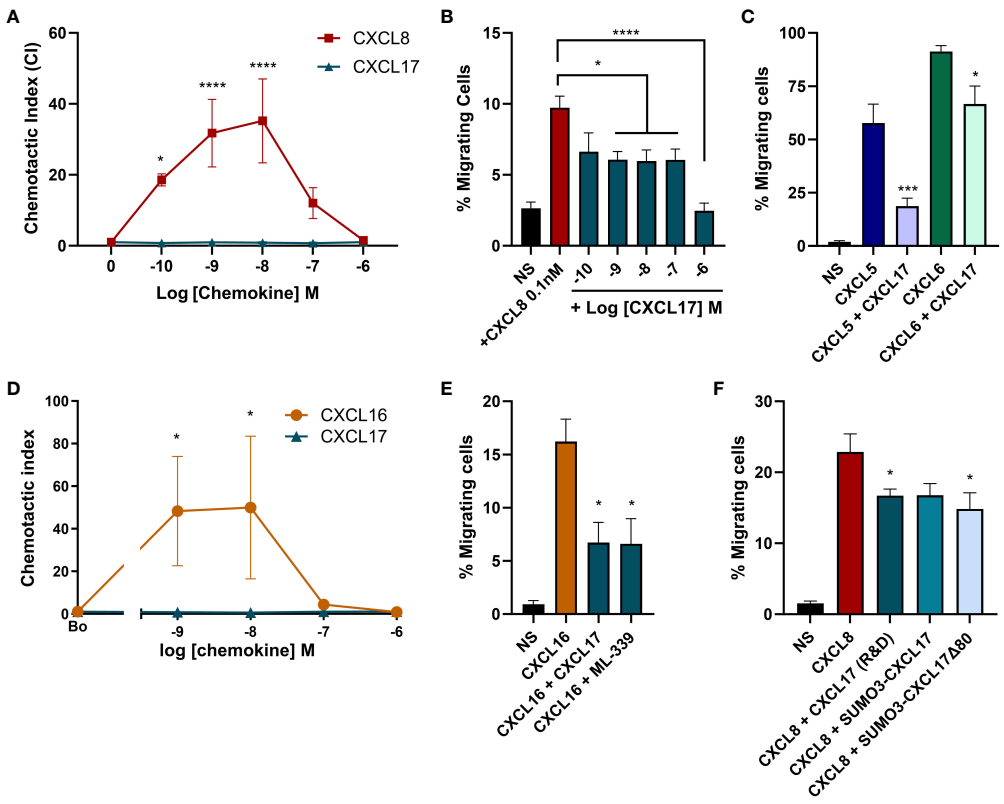

FIGURE 8
High concentrations of CXCL17 can antagonize chemotactic responses mediated by CXCR1 and CXCR6. Chemotactic responses of CXCR1 expressing Ba/F3 cells to **(A)** increasing concentrations of CXCL8 and CXCL17 (24–119) (n = 3), **(B)** CXCL8 in the presence of absence of increasing concentrations of CXCL17 (24–119) (n = 4), or **(C)** 10 nM CXCL5 and CXCL6 in the absence or presence of 1 μM CXCL17 (n = 4). Chemotactic responses of CXCR6 expressing L1.2 transfectant cells to **(D)** increasing concentrations of CXCL16 and CXCL17 (24–119) (n = 4), and to **(E)** 1 nM CXCL16 in the absence or presence of 1 μM CXCL17 or 1 μM ML-339 (n = 4). **(F)** Chemotactic responses of CXCR1-BaF/3 cells to 0.1 nM CXCL8 in the absence or presence of 1 μM CXCL17, SUMO3-CXCL17, or SUMO3-CXCL17 Δ80 (n = 4). Data are presented as mean + SEM and two-way ANOVA with multiple comparisons was performed with Fisher's LSD post-test (for **A, D**) or Dunnett's multiple comparison test (for **B, C, E, F**). Statistical significance is displayed as *p > 0.05, ***p < 0.001***, and ****p > 0.0001.

responses to CXCL17 were observed (Figure 8D). However, 1 µM CXCL17 was seen to inhibit the responses to CXCL16 with similar efficacy to 1 µM concentrations of the small-molecule CXCR6 antagonist ML-339 (Figure 8E). This suggests that while having modest chemotactic activity for many leukocyte subsets, CXCL17 has the potential to modulate the responses of a variety of chemokines.

In an attempt to address the role of GAG binding in the mechanism of inhibition, we returned our focus to CXCR1. We directly compared the ability of the truncated SUMO3-CXCL17 Δ80 construct to inhibit CXCL8 responses of CXCR1 transfectants. CXCL17 (24–119) and SUMO3-CXCL17 (24–119) were used as positive controls for inhibition. We observed robust responses of the transfectants to 0.1 nM CXCL8 (Figure 8F). Migration was significantly inhibited by CXCL17 (24–119) and a trend toward inhibition with the SUMO3-CXCL17 construct was observed, although this just failed to reach statistical significance (p = 0.0518). Interestingly, the SUMO3-CXCL17 Δ80 lacking the bulk of the CXCL17 sequence was able to significantly inhibit migration, with similar efficacy to CXCL17 (24–119). We are therefore unable to definitely conclude that interruption of GAG binding is the mechanism by which CXCL17 inhibits migration to CXCL8.

4 Discussion

CXCL17 remains a poorly characterized protein with some seemingly contradictory reports published in the literature. In this study, we showed that CXCL17 has some but not all of the properties of a chemokine. CXCL17 can form dimers like many chemokines and has relatively modest chemotactic activity, although it appears unlikely to adopt a chemokine fold. We also showed that CXCL17 is an efficacious binder to GAGs via conserved basic residues within the C-terminus. We postulate that GAG binding by CXCL17 may play a role in modulating the activity of other chemokines and facilitate the antimicrobial activity of CXCL17 at mucosal surfaces, previously reported by others.

To date, the structure of CXCL17 has not been experimentally verified, with *in silico* modeling generating contradictory reports (7–9, 62, 63). Using multiple fold prediction programs and structural modeling algorithms, our methodologies were consistent in predicting that CXCL17 is unlikely to adopt a chemokine fold. This aligns with the inability of BLAST and Pfam analysis of the CXCL17 sequence to find statistically significant structural homologs with any other characterized protein, as confirmed in an earlier report (7). The structure of CXCL17 (Q6UXB2) has been predicted by AlphaFold (Deepmind, EMBL-EBI) and found to lack structural homology with chemokines (64). However, the utility of that model may be limited due to the inclusion of the predicted N-terminal signal peptide. Using AlphaFold2 and RoseTTAFold on ColabFold, we therefore predicted the structure of the mature CXCL17 (24–119). Acknowledging the limitations of *in silico* structural modeling for proteins with few sequence homologs in reference libraries, we performed MMSeqs2 MSA of CXCL17 on 29.3 million cluster consensus sequences (35), to give the best chance of finding high-quality alignments to inform folding. ColabFold identified ~130 homologous sequences and predicted folding with AlphaFold2 (Figure 1F and Supplementary Figure 1) or RoseTTAFold (Supplementary Figures 3A–C). While the structures generated from both methods are not in agreement, they both notably lack a chemokine fold. Owing to the relatively low numbers of CXCL17 homologs in reference libraries, we additionally performed *de novo* folding in AlphaFold2 (Supplementary Figure 4) and RoseTTAFold (Supplementary Figures 3D, E) whereby the MSA step is bypassed. This approach has been reported to increase folding accuracy for proteins lacking homologs (35). A higher confidence model was generated in AlphaFold2 using this methodology (Supplementary Figure 4), as determined by PAE and plDDT scores. Inspection of the resulting *de novo* RoseTTAFold model produced a CXCL17 structure that again lacked a chemokine-like fold (Supplementary Figures 3D–F).

The lack of predicted chemokine-like homology produced by ColabFold was corroborated by C-I-TASSER modeling (Supplementary Figure 2) and supported previous I-TASSER models reported in Giblin and Pease (9), Sun et al. (62), and Nijja et al. (63), although in the latter two articles, no discussion of the lack of a chemokine-like structure for CXCL17 was made by the authors. The relatively low confidence of the C-I-TASSER models indicates low significance of threading template alignments due to a lack of experimentally verified homologs, which, itself, speaks to the low conservation between CXCL17 and all other chemokines. Perhaps the generation of several non-chemokine-like structural predictions for CXCL17 is unsurprising, given that the N-terminally extended region of CXCL17 with its two CXC motifs is not conducive to alignment with other CXC-chemokines. One likely flaw in the initial prediction of Pisabarro et al. is the usage of a limited quality of homologs (7,950 PDB library entries) of which the 6th and 12th ranked proteins (CCL3: 16.2% identity) and CXCL8 (14.3% identity) were used to generate a new fold library containing all known CXCL8 mutants at that time (7). Notably, CXCL17 was postulated to form a chemokine fold resembling that of the CXCL8 Glu38Cys/Cys50Ala mutant (1ICW), which was deliberately engineered to modify the disulfide bonding of the chemokine with deleterious effects on receptor binding (65). Significantly, by their own confidence criteria, other proteins in the library with higher homology were ignored, such as the RXR-α DNA-binding domain (1dsz.B) for which the solved structure comprises of a zinc-stabilized bundle of 3 α-helices with a short length of antiparallel β-strand (66). The helical portions of the RXR-α DNA-binding domain protein are in fact more consistent with *in silico* generated models of CXCL17 presented here. In conclusion, we find no evidence to support the likelihood of CXCL17 adopting a chemokine-like fold. Experimental verification of the CXCL17 structure by 2D-NMR or crystallography is required to provide a definitive answer to the structural basis for classifying CXCL17 as a chemokine.

Chemokines are noted for their propensity to form higher-order oligomers as a function of increasing concentration (67). Early efforts in the field were made by groups to generate mutant forms of chemokines less prone to oligomerization, for example, the BB-10010 form of CCL3. By virtue of an Asp26-Ala mutation, the BB-

10010 variant of CCL3 has greatly increased solubility, facilitating its clinical evaluation as a mobilizing agent of stem cells (68). Here, we show that recombinant CXCL17 expressed in either prokaryotic or eukaryotic systems readily forms dimers as revealed by the apparent molecular weight on Western blot. ColabFold modeling suggests that the CXCL17 dimer interface is likely to be at their C-termini, although as with the CXCL17 monomer, these models require structural verification. A wider point illuminated by our observation is that a reinterpretation of a previous study regarding the potential for proteolytic cleavage of CXCL17 may be in order. Lee et al. previously reported that CXCL17 expressed by cells from the rat stomach ran as proteins of approximately 8 kDa and 22 kDa as visualized by SDS-PAGE/Western blotting (17). These data were corroborated using HEK-293T cells expressing human CXCL17 (1–119). The authors of that study interpreted their observation as being evident of the post-translational cleavage of a larger CXCL17 pro-protein into a smaller CXCL17 (64–119) form. They suggested that three basic residues between the second and third cysteines of CXCL17 were the likely site of cleavage and went on to show that expression of a mutant CXCL17 (1–119) in which the tribasic motif was mutated to alanine resulted in expression only of the 22-kDa species. A more feasible explanation in our opinion is that the two species of CXCL17 represents monomer and dimer variants of CXCL17 (24–119). Such an interpretation would also fit better with the apparent molecule weights of the CXCL17 forms on SDS-PAGE. The apparent failure of the Lys61–Arg63 triple alanine mutant of CXCL17 (1–119) to undergo cleavage may be explained by the possibility that the mutation tips the balance in favor of CXCL17 dimer formation (17).

In a similar fashion, although CXCL17 was originally described as a dendritic and monocytic cell chemoattractant protein (7), supporting data from other groups describing chemoattractant properties for CXCL17 are mixed. Notably, GPR35 was previously postulated to be a receptor for CXCL17 (21), which has been questioned by other groups, including our own (22, 23). A study by Matsui and colleagues suggested that mouse CXCL17 (23–117) was chemotactic for splenocytes with optimum migration observed at a concentration approximately 20 nM, an order of magnitude more potent than the previously described activity of human CXCL17 for monocytes and dendritic cells (7, 19). However, we were unable to reproduce these findings. While the splenocyte T-cell, B-cell, neutrophil and monocyte fractions responded to CXCL12, no significant chemotaxis to a broad range of CXCL17 concentrations was observed above the basal response. We note that Matsui and colleagues used splenocytes isolated from SCID mice whereas our splenocytes were isolated from wild-type C57BL/6 mice, so perhaps this biological difference may explain our divergent findings.

Using the TAXIScan system, we observed that human CXCL17 (24–119) was chemotactic for human neutrophils, which, to our knowledge, is the first report of CXCL17 recruiting this leukocyte population. However, this activity was weak, with significant chemotaxis only observed at CXCL17 concentrations 500-fold higher than the CXCL8 positive control. CXCL8 activates both CXCR1 and CXCR2 on neutrophils, a property it shares with several other CXC chemokines containing an ELR motif (Glutamate–Leucine–Arginine) upstream of the CXC sequence. The lack of an ELR motif within the CXCL17 sequence, coupled with the weak chemotactic activity for neutrophils, suggest that these responses are mediated by a receptor other than CXCR1 or CXCR2. The CXCL17 (24–119) form has a greatly extended N-terminus when compared to other CXC chemokines, which is hard to reconcile with current models of chemokine receptor activation (69, 70). In these models, a relatively short N-terminus inserts into the helical bundle to induce the conformation changes required for productive G protein coupling. The generation of a CXCL17 (64–119) form postulated by Lee and colleagues, although having four cysteine residues like most other CXC chemokines, is unlikely to adopt a chemokine-like fold; therefore, any chemotaxis is likely to be mediated via a mechanism atypical of CXC chemokines (70). Perhaps tellingly, the functional validation of commercially available recombinant CXCL17 (24–119) from a variety of sources does not report chemotactic activity for leukocytes but the ability to induce VEGF expression in mouse endothelial cells (49). This leads us to conclude that the primary biological function of CXCL17 may not be to promote leukocyte chemotaxis.

Using solid-phase and BLI-based assays, we report that CXCL17 binds with high affinity to a variety of GAGs, as may be predicted given the high proportion of basic residues within the primary sequence. Direct comparisons with the well-characterized GAG-binding chemokine CXCL4 (48) found that CXCL17 bound to GAGs with comparably high capacity, often exceeding that of CXCL4. Additionally, CXCL4 and CXCL17 had similar dissociation rates from heparin and HS, which may be indicative of comparable binding affinities. In contrast to CXCL4, reduction of the disulfide bonds within CXCL17 had negligible effect upon GAG binding, suggesting that tertiary conformation plays little role in CXCL17-GAG binding. Serial truncation of CXCL17 revealed that a BBXB and BXXBB motif conserved between residues 85 and 98 appeared to be a major determinant for binding to HS and chondroitin sulfate. Taken together with the observation that CXCL17 can form dimers, it suggests that CXCL17 dimers may form on GAGs as a function of increasing CXCL17 concentration. So what might be the function of GAG-bound CXCL17? Since constitutive expression of CXCL17 is restricted to gastric and respiratory mucosal tissues, CXCL17 expressed at such locations is perfectly placed to bind with strong affinity to GAGs present either in free forms or bound to cells. Such a process may permit the retention and oligomerization of CXCL17 on mucosal surfaces to create high local concentrations at pathogen infection routes. Given reports of bactericidal and fungicidal activity against a variety of pathogens (16), GAG-bound CXCL17 is likely to form a first line of defense against microbes. Consistent with such a function, CXCL17 expression by epithelial cells has been reported to be induced following challenge of mice with Mycobacteria, although CXCL17-deficient mice were found to be no more susceptible to infection than wild-type littermates (71). CXCL17-deficient mice have also been reported to be less resistant to infection in a mouse model of herpes simplex virus infection, although this was postulated to be a result of impaired trafficking of $GPR35^{+}$ cytotoxic T cells (72).

Mechanistically, cationic antimicrobial proteins exert their effects by associating to negatively charged lipopolysaccharides

(LPS) on Gram-negative bacterial membranes, where they introduce transient membrane defects or form stable pore complexes to permeate the membrane, killing the pathogen [reviewed in (18, 73, 74)]. Burkhardt et al. previously reported that CXCL17 exerts its antimicrobial effects on *E. coli* by permeabilizing the bacterial membrane, and rightly speculated with the available structural models for CXCL17 at the time that due to the constraints of the general chemokine structure, the antimicrobial mechanism of action must differ from that of other linear antimicrobial peptides and defensins (16, 75, 76). Here, we provide evidence that the structure of CXCL17 is unlikely to be constrained in this manner and therefore raise the possibility that CXCL17 may partly function as a monomeric or dimeric pore-forming antimicrobial protein, a question that may now merit further investigation. Interestingly, the fungicidal activity of CXCL17 suggests that it also has the capacity to permeabilize eukaryotic cell membranes, which could potentially be mediated by the charged carboxyl tail as similarly described for CCL28 (77).

Additionally, via the same electrostatic mechanisms by which CXCL17 is likely to associate to bacterial membranes, the cationic residues within CXCL17 may permit binding of LPS, thereby dampening innate immune responses originating in the mucosae. Moderately high concentrations of CXCL17 (300 nM) were shown to significantly reduce LPS-induced transcription of inflammatory markers IL-6, TNFα, and iNOS in macrophages *in vitro*, in a manner that was enhanced by priming the cells in the presence of CXCL17 overnight (17). While no mechanism was proposed for this inflammation suppressing effect at the time, cell surface GAG-bound CXCL17 could be envisaged to bind free LPS or remodel the macrophage glycocalyx to fine-tune TLR4-mediated responses.

Contrary to previous reports of chemotactic activity assigned to CXCL17, we could only demonstrate weak agonist activity for human neutrophils and failed to see convincing migratory responses of murine splenocytes. Previously, we and others have struggled to show robust chemotactic activity for monocytes and THP-1 cells using a commercially available CXCL17 (24–119) form (22, 23). We therefore assumed that CXCL17 might play another physiological role. Indeed, at micromolar concentrations of CXCL17, we observed the disruption of chemotactic responses of CXCR1 transfectants to CXCL5, CXCL6, and CXCL8. A similar inhibitory observation was recently reported for the CXCL12–CXCR4 signaling axis (78), suggesting that CXCL17 may have broadly inhibitory effects on the function of a variety of chemokines and may serve to moderate chemokine signaling *in vivo*. This is also supported by our observations that chemotactic responses of CXCR6 transfectants to CXCL16 were also inhibited by the CXCL17 (24–119) form. A lack of such inhibition may explain, in part, the perturbed trafficking of lymphoid and myeloid cells and exacerbated disease reported in CXCL17-deficient mice utilized in a model of experimental autoimmune encephalomyelitis (EAE) (79).

We postulate that the mechanism of action underlying inhibition of chemotaxis may be due to competition for cell-surface GAGs on the migrating cell, since we have previously reported that GAG binding is a requirement for chemotactic responses to CXCL8 (44). Our attempts in this study to directly link GAG binding of CXCL17 to inhibition of chemotaxis using CXCL17 C-truncation were unsuccessful, since the SUMO3-CXCL17 Δ80 construct retained significant inhibitory activity. With hindsight, this might have been anticipated, since the construct still retained substantial heparin binding capacity, albeit reduced from full-length CXCL17. Notably, this SUMO3-CXCL17 Δ80 construct contained an N-terminal BXB motif, which may still facilitate binding to GAGs. We envisage that in these assays, the anchoring of the relatively large SUMO3 proteins to cell surface GAGs may be sterically hindering the interaction of chemokines with receptors. Future studies using GAG binding-deficient point mutants of CXCL17 (24–119), devoid of an N-terminal fusion partner, may help to clarify the inhibitory mechanism.

We can also speculate that while disrupting inappropriate pro-inflammatory signals originating in the gastric and respiratory mucosa, CXCL17 may still permit the transmigration of leukocytes via receptor-independent GAG-mediated interactions as recently described for CXCL4 (56), potentially by condensing cell-associated HS proteoglycans to generate a denser glycocalyx and promote cell-surface interactions with the local extracellular matrix; thus, while inappropriate anti-commensal immune responses may be dampened, tissue homoeostasis and immune sensing of the microbiome may still take place by patrolling leukocytes.

In summary, we report that CXCL17 displays some but not all the properties associated with a chemokine. CXCL17 has only feeble chemoattractant properties for human neutrophils, which may be due to the adoption of a protein fold not consistent with other members of the chemokine family. However, like some other chemokines, CXCL17 has a tendency to form dimers and is an efficacious binder to a variety of GAGs. GAG binding may enhance the antimicrobial of CXCL17 at mucosal surfaces, and it is possible that CXCL17 modulates the function of other chemokines dependent on interactions with GAGs for their signaling. Peptides derived from the CXCL17 sequence may therefore have immunomodulatory functions as has been exploited by others, for example, C-terminal derivatives of CXCL9 (80–83). As such, CXCL17 may prove to be a useful tool with which to modulate a variety of inflammatory processes.

Data availability statement

The raw data supporting the conclusions of this article will be made available by the authors, without undue reservation.

Ethics statement

The studies involving humans were approved by Imperial College Healthcare Tissue Bank. The studies were conducted in accordance with the local legislation and institutional requirements. The participants provided their written informed consent to participate in this study. The animal study was approved by the Home Office of Great Britain, in accordance with the recommendations in the Guide for the Use of Laboratory

Animals of Imperial College London, with the ARRIVE (Animal Research: Reporting of *In Vivo* Experiments) guidelines. All animal procedures and care conformed strictly to the UK Home Office Guidelines under the Animals (Scientific Procedures) Act 1986. The study was conducted in accordance with the local legislation and institutional requirements.

Author contributions

SG: Formal Analysis, Investigation, Supervision, Writing – original draft, Writing – review & editing. SR: Investigation, Writing – review & editing. SH: Investigation, Writing – review & editing. HB: Formal Analysis, Investigation, Writing – review & editing. KM: Resources, Writing – review & editing. RS: Funding acquisition, Resources, Writing – review & editing. TT: Resources, Writing – review & editing. SK: Resources, Writing – review & editing. DD: Resources, Writing – review & editing. JP: Conceptualization, Funding acquisition, Investigation, Supervision, Writing – review & editing.

Funding

This research was supported by the Wellcome Trust (Collaborative Award 215539, JP). For the purpose of open access, the authors have applied a Creative Commons Attribution (CC BY) license to any Author Accepted Manuscript version arising. The authors acknowledge financial support from Imperial College London through an Imperial College Research Fellowship grant awarded to KM. RS is a Wellcome Trust Senior Research Fellow in Basic Biomedical Sciences (209458/Z/17/Z). DD was supported by a Sir Henry Dale fellowship jointly funded by the Wellcome Trust and the Royal Society (Grant Number 218570/Z/19/Z), and a Wellcome Trust centre grant (Grant Number 203128/A/16/Z).

Conflict of interest

The authors declare that the research was conducted in the absence of any commercial or financial relationships that could be construed as a potential conflict of interest.

Publisher's note

Supplementary material

The Supplementary Material for this article can be found online at: https://www.frontiersin.org/articles/10.3389/fimmu.2023.1254697/full#supplementary-material

References

1. Zlotnik A, Yoshie O. The chemokine superfamily revisited. *Immunity* (2012) 36:705–16. doi: 10.1016/j.immuni.2012.05.008

2. St Charles R, Walz DA, Edwards BF. The three-dimensional structure of bovine platelet factor 4 at 3.0-A resolution. *J Biol Chem* (1989) 264:2092–9. doi: 10.1016/S0021-9258(18)94146-3

3. Zlotnik A, Yoshie O, Nomiyama H. The chemokine and chemokine receptor superfamilies and their molecular evolution. *Genome Biol* (2006) 7:243. doi: 10.1186/gb-2006-7-12-243

4. Murphy PM, Baggiolini M, Charo IF, Hebert CA, Horuk R, Matsushima K, et al. International union of pharmacology. XXII. Nomenclature for chemokine receptors. *Pharmacol Rev* (2000) 52:145–76.

5. Murphy PM. International Union of Pharmacology. XXX. Update on chemokine receptor nomenclature. *Pharmacol Rev* (2002) 54:227–9. doi: 10.1124/pr.54.2.227

6. Bachelerie F, Ben-Baruch A, Burkhardt AM, Combadiere C, Farber JM, Graham GJ, et al. International Union of Basic and Clinical Pharmacology. [corrected]. LXXXIX. Update on the extended family of chemokine receptors and introducing a new nomenclature for atypical chemokine receptors. *Pharmacol Rev* (2014) 66:1–79. doi: 10.1124/pr.113.007724

7. Pisabarro MT, Leung B, Kwong M, Corpuz R, Frantz GD, Chiang N, et al. Cutting edge: novel human dendritic cell- and monocyte-attracting chemokine-like protein identified by fold recognition methods. *J Immunol* (2006) 176:2069–73. doi: 10.4049/jimmunol.176.4.2069

8. Denisov SS. CXCL17: the black sheep in the chemokine flock. *Front Immunol* (2021) 12:712897. doi: 10.3389/fimmu.2021.712897

9. Giblin SP, Pease JE. What defines a chemokine? - The curious case of CXCL17. *Cytokine* (2023) 168:156224. doi: 10.1016/j.cyto.2023.156224

10. Matloubian M, David A, Engel S, Ryan JE, Cyster JG. A transmembrane CXC chemokine is a ligand for HIV-coreceptor Bonzo. *Nat Immunol* (2000) 1:298–304. doi: 10.1038/79738

11. Miller MD, Wilson SD, Dorf ME, Seuanez HN, O'Brien SJ, Krangel MS. Sequence and chromosomal location of the I-309 gene. Relationship to genes encoding a family of inflammatory cytokines. *J Immunol* (1990) 145:2737–44. doi: 10.4049/jimmunol.145.8.2737

12. Pardigol A, Forssmann U, Zucht HD, Loetscher P, Schulz-Knappe P, Baggiolini M, et al. HCC-2, a human chemokine: gene structure, expression pattern, and biological activity. *Proc Natl Acad Sci U.S.A.* (1998) 95:6308–13. doi: 10.1073/pnas.95.11.6308

13. Hedrick JA, Zlotnik A. Identification and characterization of a novel beta chemokine containing six conserved cysteines. *J Immunol* (1997) 159:1589–93. doi: 10.4049/jimmunol.159.4.1589

14. Patel VP, Kreider BL, Li Y, Li H, Leung K, Salcedo T, et al. Molecular and functional characterization of two novel human C-C chemokines as inhibitors of two distinct classes of myeloid progenitors. *J Exp Med* (1997) 185:1163–72. doi: 10.1084/jem.185.7.1163

15. Wang W, Soto H, Oldham ER, Buchanan ME, Homey B, Catron D, et al. Identification of a novel chemokine (CCL28), which binds CCR10 (GPR2). *J Biol Chem* (2000) 275:22313–23. doi: 10.1074/jbc.M001461200

16. Burkhardt AM, Tai KP, Flores-Guiterrez JP, Vilches-Cisneros N, Kamdar K, Barbosa-Quintana O, et al. CXCL17 is a mucosal chemokine elevated in idiopathic pulmonary fibrosis that exhibits broad antimicrobial activity. *J Immunol* (2012) 188:6399–406. doi: 10.4049/jimmunol.1102903

17. Lee WY, Wang CJ, Lin TY, Hsiao CL, Luo CW. CXCL17, an orphan chemokine, acts as a novel angiogenic and anti-inflammatory factor. *Am J Physiol Endocrinol Metab* (2013) 304:E32–40. doi: 10.1152/ajpendo.00083.2012

18. Yung SC, Murphy PM. Antimicrobial chemokines. *Front Immunol* (2012) 3:276. doi: 10.3389/fimmu.2012.00276

19. Matsui A, Yokoo H, Negishi Y, Endo-Takahashi Y, Chun NA, Kadouchi I, et al. CXCL17 expression by tumor cells recruits CD11b+Gr1 high F4/80- cells and promotes tumor progression. *PloS One* (2012) 7:e44080. doi: 10.1371/journal.pone.0044080

20. Burkhardt AM, Maravillas-Montero JL, Carnevale CD, Vilches-Cisneros N, Flores JP, Hevezi PA, et al. CXCL17 is a major chemotactic factor for lung macrophages. *J Immunol* (2014) 193:1468–74.

21. Maravillas-Montero JL, Burkhardt AM, Hevezi PA, Carnevale CD, Smit MJ, Zlotnik A. Cutting edge: GPR35/CXCR8 is the receptor of the mucosal chemokine CXCL17. *J Immunol* (2015) 194:29–33. doi: 10.4049/jimmunol.1401704

22. Park SJ, Lee SJ, Nam SY, Im DS. GPR35 mediates lodoxamide-induced migration inhibitory response but not CXCL17-induced migration stimulatory response in THP-1 cells; is GPR35 a receptor for CXCL17? *Br J Pharmacol* (2018) 175:154–61. doi: 10.1111/bph.14082

23. Binti Mohd Amir NAS, Mackenzie AE, Jenkins L, Boustani K, Hillier MC, Tsuchiya T, et al. Evidence for the existence of a CXCL17 receptor distinct from GPR35. *J Immunol* (2018) 201:714–24. doi: 10.4049/jimmunol.1700884

24. De Giovanni M, Tam H, Valet C, Xu Y, Looney MR, Cyster JG. GPR35 promotes neutrophil recruitment in response to serotonin metabolite 5-HIAA. *Cell* (2022) 185:815–830 e19. doi: 10.1016/j.cell.2022.01.010

25. Proudfoot AE. The biological relevance of chemokine-proteoglycan interactions. *Biochem Soc Trans* (2006) 34:422–6. doi: 10.1042/BST0340422

26. Proudfoot AEI, Johnson Z, Bonvin P, Handel TM. Glycosaminoglycan interactions with chemokines add complexity to a complex system. *Pharm (Basel)* (2017) 10. doi: 10.3390/ph10030070

27. Crijns H, Vanheule V, Proost P. Targeting chemokine-glycosaminoglycan interactions to inhibit inflammation. *Front Immunol* (2020) 11:483. doi: 10.3389/fimmu.2020.00483

28. Sutherland TE, Dyer DP, Allen JE. The extracellular matrix and the immune system: A mutually dependent relationship. *Science* (2023) 379:eabp8964. doi: 10.1126/science.abp8964

29. Teufel F, Almagro Armenteros JJ, Johansen AR, Gislason MH, Pihl SI, Tsirigos KD, et al. SignalP 6.0 predicts all five types of signal peptides using protein language models. *Nat Biotechnol* (2022) 40:1023–5. doi: 10.1038/s41587-021-01156-3

30. Madeira F, Pearce M, Tivey ARN, Basutkar P, Lee J, Edbali O, et al. Search and sequence analysis tools services from EMBL-EBI in 2022. *Nucleic Acids Res* (2022) 50:W276–9. doi: 10.1093/nar/gkac240

31. Letunic I, Bork P. Interactive Tree Of Life (iTOL) v5: an online tool for phylogenetic tree display and annotation. *Nucleic Acids Res* (2021) 49:W293–6. doi: 10.1093/nar/gkab301

32. Combet C, Blanchet C, Geourjon C, Deléage G. NPS@: network protein sequence analysis. *Trends Biochem Sci* (2000) 25:147–50. doi: 10.1016/S0968-0004(99)01540-6

33. Gupta R, Brunak S. Prediction of glycosylation across the human proteome and the correlation to protein function. *Pac Symp Biocomput* (2002) 7:310–22.

34. Steentoft C, Vakhrushev SY, Joshi HJ, Kong Y, Vester-Christensen MB, Schjoldager KT, et al. Precision mapping of the human O-GalNAc glycoproteome through SimpleCell technology. *EMBO J* (2013) 32:1478–88. doi: 10.1038/emboj.2013.79

35. Mirdita M, Schutze K, Moriwaki Y, Heo L, Ovchinnikov S, Steinegger M. ColabFold: making protein folding accessible to all. *Nat Methods* (2022) 19:679–82. doi: 10.1038/s41592-022-01488-1

36. Tunyasuvunakool K, Adler J, Wu Z, Green T, Zielinski M, Zidek A, et al. Highly accurate protein structure prediction for the human proteome. *Nature* (2021) 596:590–6. doi: 10.1038/s41586-021-03828-1

37. Varadi M, Anyango S, Deshpande M, Nair S, Natassia C, Yordanova G, et al. AlphaFold Protein Structure Database: massively expanding the structural coverage of protein-sequence space with high-accuracy models. *Nucleic Acids Res* (2022) 50:D439–44. doi: 10.1093/nar/gkab1061

38. Zheng W, Li Y, Zhang C, Pearce R, Mortuza SM, Zhang Y. Deep-learning contact-map guided protein structure prediction in CASP13. *Proteins* (2019) 87:1149–64. doi: 10.1002/prot.25792

39. Allen SJ, Hamel DJ, Handel TM. A rapid and efficient way to obtain modified chemokines for functional and biophysical studies. *Cytokine* (2011) 55:168–73. doi: 10.1016/j.cyto.2011.05.002

40. McKenna S, Giblin SP, Bunn RA, Xu Y, Matthews SJ, Pease JE. A highly efficient method for the production and purification of recombinant human CXCL8. *PloS One* (2021) 16:e0258270. doi: 10.1371/journal.pone.0258270

41. Veldkamp CT, Koplinski CA, Jensen DR, Peterson FC, Smits KM, Smith BL, et al. Production of recombinant chemokines and validation of refolding. *Methods Enzymol* (2016) 570:539–65. doi: 10.1016/bs.mie.2015.09.031

42. Cockett MI, Bebbington CR, Yarranton GT. The use of engineered E1A genes to transactivate the hCMV-MIE promoter in permanent CHO cell lines. *Nucleic Acids Res* (1991) 19:319–25. doi: 10.1093/nar/19.2.319

43. Vaidehi N, Pease JE, Horuk R. Modeling small molecule-compound binding to G-protein-coupled receptors. *Methods Enzymol* (2009) 460:263–88. doi: 10.1016/S0076-6879(09)05213-6

44. Goldblatt J, Lawrenson RA, Muir L, Dattani S, Hoffland A, Tsuchiya T, et al. A requirement for neutrophil glycosaminoglycans in chemokine:Receptor interactions is revealed by the streptococcal protease spyCEP. *J Immunol* (2019) 202:3246–55. doi: 10.4049/jimmunol.1801688

45. Zengel P, Nguyen-Hoang A, Schildhammer C, Zantl R, Kahl V, Horn E. mu-Slide Chemotaxis: a new chamber for long-term chemotaxis studies. *BMC Cell Biol* (2011) 12:21. doi: 10.1186/1471-2121-12-21

46. Salanga CL, Dyer DP, Kiselar JG, Gupta S, Chance MR, Handel TM. Multiple glycosaminoglycan-binding epitopes of monocyte chemoattractant protein-3/CCL7 enable it to function as a non-oligomerizing chemokine. *J Biol Chem* (2014) 289:14896–912. doi: 10.1074/jbc.M114.547737

47. Dyer DP, Salanga CL, Johns SC, Valdambrini E, Fuster MM, Milner CM, et al. The anti-inflammatory protein TSG-6 regulates chemokine function by inhibiting chemokine/glycosaminoglycan interactions. *J Biol Chem* (2016) 291:12627–40. doi: 10.1074/jbc.M116.720953

48. Dyer DP, Salanga CL, Volkman BF, Kawamura T, Handel TM. The dependence of chemokine-glycosaminoglycan interactions on chemokine oligomerization. *Glycobiology* (2016) 26:312–26. doi: 10.1074/jbc.M116.720953

49. Weinstein EJ, Head R, Griggs DW, Sun D, Evans RJ, Swearingen ML, et al. VCC-1, a novel chemokine, promotes tumor growth. *Biochem Biophys Res Commun* (2006) 350:74–81. doi: 10.1016/j.bbrc.2006.08.194

50. Wilbanks A, Zondlo SC, Murphy K, Mak S, Soler D, Langdon P, et al. Expression cloning of the STRL33/BONZO/TYMSTRligand reveals elements of CC, CXC, and CX3C chemokines. *J Immunol* (2001) 166:5145–54. doi: 10.4049/jimmunol.166.8.5145

51. Pease JE, Williams TJ. The attraction of chemokines as a target for specific anti-inflammatory therapy. *Br J Pharmacol* (2006) 147(Suppl 1):S212–21. doi: 10.1038/sj.bjp.0706475

52. Nitta N, Tsuchiya T, Yamauchi A, Tamatani T, Kanegasaki S. Quantitative analysis of eosinophil chemotaxis tracked using a novel optical device – TAXIScan. *J Immunol Methods* (2007) 320:155–63. doi: 10.1016/j.jim.2006.12.010

53. Handel TM, Dyer DP. Perspectives on the biological role of chemokine: Glycosaminoglycan interactions. *J Histochem Cytochem* (2021) 69:87–91. doi: 10.1369/0022155420977971

54. Dyer DP, Thomson JM, Hermant A, Jowitt TA, Handel TM, Proudfoot AE, et al. TSG-6 inhibits neutrophil migration *via* direct interaction with the chemokine CXCL8. *J Immunol* (2014) 192:2177–85. doi: 10.4049/jimmunol.1300194

55. Deuel TF, Keim PS, Farmer M, Heinrikson RL. Amino acid sequence of human platelet factor 4. *Proc Natl Acad Sci U.S.A.* (1977) 74:2256–8. doi: 10.1073/pnas.74.6.2256

56. Gray AL, Karlsson R, Roberts ARE, Ridley AJL, Pun N, Khan B, et al. Chemokine CXCL4 interactions with extracellular matrix proteoglycans mediate widespread immune cell recruitment independent of chemokine receptors. *Cell Rep* (2023) 42:111930. doi: 10.1016/j.celrep.2022.111930

57. Shah NB, Duncan TM. Bio-layer interferometry for measuring kinetics of protein-protein interactions and allosteric ligand effects. *J Vis Exp* (2014) (84):e51383. doi: 10.3791/51383

58. Schuck P, Zhao H. The role of mass transport limitation and surface heterogeneity in the biophysical characterization of macromolecular binding processes by SPR biosensing. *Methods Mol Biol* (2010) 627:15–54. doi: 10.1007/978-1-60761-670-2_2

59. Svitel J, Boukari H, Van Ryk D, Willson RC, Schuck P. Probing the functional heterogeneity of surface binding sites by analysis of experimental binding traces and the effect of mass transport limitation. *Biophys J* (2007) 92:1742–58. doi: 10.1529/biophysj.106.094615

60. Dyer DP, Migliorini E, Salanga CL, Thakar D, Handel TM, Richter RP. Differential structural remodelling of heparan sulfate by chemokines: the role of chemokine oligomerization. *Open Biol* (2017) 7:160286. doi: 10.1098/rsob.160286

61. Handel TM, Johnson Z, Crown SE, Lau EK, Proudfoot AE. Regulation of protein function by glycosaminoglycans–as exemplified by chemokines. *Annu Rev Biochem* (2005) 74:385–410. doi: 10.1146/annurev.biochem.72.121801.161747

62. Sun C, Shen H, Cai H, Zhao Z, Gan G, Feng S, et al. Intestinal guard: Human CXCL17 modulates protective response against mycotoxins and CXCL17-mimetic peptides development. *Biochem Pharmacol* (2021) 188:114586. doi: 10.1016/j.bcp.2021.114586

63. Niiya K, Ohara H, Isono M, Sheikh AM, Matsuo H, Fujikawa K, et al. Further dissection of QTLs for salt-induced stroke and identification of candidate genes in the stroke-prone spontaneously hypertensive rat. *Sci Rep* (2018) 8:9403. doi: 10.1038/s41598-018-27539-2

64. Jumper J, Evans R, Pritzel A, Green T, Figurnov M, Ronneberger O, et al. Highly accurate protein structure prediction with AlphaFold. *Nature* (2021) 596:583–9. doi: 10.1038/s41586-021-03819-2

65. Eigenbrot C, Lowman HB, Chee L, Artis DR. Structural change and receptor binding in a chemokine mutant with a rearranged disulfide: X-ray structure of E38C/C50AIL-8 at 2 A resolution. *Proteins* (1997) 27:556–66. doi: 10.1002/(SICI)1097-0134(199704)27:4<556::AID-PROT8>3.0.CO;2-8

66. Rastinejad F, Wagner T, Zhao Q, Khorasanizadeh S. Structure of the RXR-RAR DNA-binding complex on the retinoic acid response element DR1. *EMBO J* (2000) 19:1045–54. doi: 10.1093/emboj/19.5.1045

67. Salanga CL, Handel TM. Chemokine oligomerization and interactions with receptors and glycosaminoglycans: the role of structural dynamics in function. *Exp Cell Res* (2011) 317:590–601. doi: 10.1016/j.yexcr.2011.01.004

68. Hunter MG, Bawden L, Brotherton D, Craig S, Cribbes S, Czaplewski LG, et al. BB-10010: an active variant of human macrophage inflammatory protein-1 alpha with improved pharmaceutical properties. *Blood* (1995) 86:4400–8. doi: 10.1182/blood.V86.12.4400.bloodjournal86124400

69. Kufareva I, Gustavsson M, Zheng Y, Stephens BS, Handel TM. What do structures tell us about chemokine receptor function and antagonism? *Annu Rev Biophys* (2017) 46:175–98. doi: 10.1146/annurev-biophys-051013-022942

70. Kleist AB, Getschman AE, Ziarek JJ, Nevins AM, Gauthier PA, Chevigne A, et al. New paradigms in chemokine receptor signal transduction: Moving beyond the two-site model. *Biochem Pharmacol* (2016) 114:53–68. doi: 10.1016/j.bcp.2016.04.007

71. Choreno-Parra JA, Dunlap MD, Swanson R, Jimenez-Alvarez LA, Munoz-Torrico M, Guzman-Beltran S, et al. CXCL17 Is Dispensable during Hypervirulent Mycobacterium tuberculosis HN878 Infection in Mice. *Immunohorizons* (2021) 5:752–9. doi: 10.4049/immunohorizons.2100048

72. Srivastava R, Hernandez-Ruiz M, Khan AA, Fouladi MA, Kim GJ, Ly VT, et al. CXCL17 chemokine-dependent mobilization of CXCR8(+)CD8(+) effector memory and tissue-resident memory T cells in the vaginal mucosa is associated with protection against genital herpes. *J Immunol* (2018) 200:2915–26. doi: 10.4049/jimmunol.1701474

73. Huan Y, Kong Q, Mou H, Yi H. Antimicrobial peptides: classification, design, application and research progress in multiple fields. *Front Microbiol* (2020) 11:582779. doi: 10.3389/fmicb.2020.582779

74. Lei J, Sun L, Huang S, Zhu C, Li P, He J, et al. The antimicrobial peptides and their potential clinical applications. *Am J Transl Res* (2019) 11:3919–31.

75. Hristova K, Selsted ME, White SH. Interactions of monomeric rabbit neutrophil defensins with bilayers: comparison with dimeric human defensin HNP-2. *Biochemistry* (1996) 35:11888–94. doi: 10.1021/bi961100d

76. Lehrer RI, Lu W. alpha-Defensins in human innate immunity. *Immunol Rev* (2012) 245:84–112. doi: 10.1111/j.1600-065X.2011.01082.x

77. He J, Thomas MA, de Anda J, Lee MW, Van Why E, Simpson P, et al. Chemokine CCL28 is a potent therapeutic agent for oropharyngeal candidiasis. *Antimicrob Agents Chemother* (2020) 64:e00210-20. doi: 10.1128/AAC.00210-20

78. White CW, Kilpatrick LE, Dale N, Abhayawardana RS, Dekkers S, Stocks MJ, et al. CXCL17 is an endogenous inhibitor of CXCR4 *via* a novel mechanism of action. *bioRxiv* (2021). doi: 10.1101/2021.07.05.451109

79. Hernandez-Ruiz M, Othy S, Herrera C, Nguyen HT, Arrevillaga-Boni G, Catalan-Dibene J, et al. Cxcl17(-/-) mice develop exacerbated disease in a T cell-dependent autoimmune model. *J Leukoc Biol* (2019) 105:1027–39. doi: 10.1002/JLB.3A0918-345RR

80. Boff D, Crijns H, Janssens R, Vanheule V, Menezes GB, Macari S, et al. The chemokine fragment CXCL9(74-103) diminishes neutrophil recruitment and joint inflammation in antigen-induced arthritis. *J Leukoc Biol* (2018) 104:413–22. doi: 10.1002/JLB.3MA1217-502R

81. Vanheule V, Boff D, Mortier A, Janssens R, Petri B, Kolaczkowska E, et al. CXCL9-derived peptides differentially inhibit neutrophil migration *in vivo* through interference with glycosaminoglycan interactions. *Front Immunol* (2017) 8:530. doi: 10.3389/fimmu.2017.00530

82. Vanheule V, Janssens R, Boff D, Kitic N, Berghmans N, Ronsse I, et al. The positively charged COOH-terminal glycosaminoglycan-binding CXCL9(74-103) peptide inhibits CXCL8-induced neutrophil extravasation and monosodium urate crystal-induced gout in mice. *J Biol Chem* (2015) 290:21292–304. doi: 10.1074/jbc.M115.649855

83. De Zutter A, Crijns H, Berghmans N, Garcia-Caballero M, Vanbrabant L, Portner N, et al. The chemokine-based peptide, CXCL9(74-103), inhibits angiogenesis by blocking heparan sulfate proteoglycan-mediated signaling of multiple endothelial growth factors. *Cancers (Basel)* (2021) 13:5090. doi: 10.3390/cancers13205090